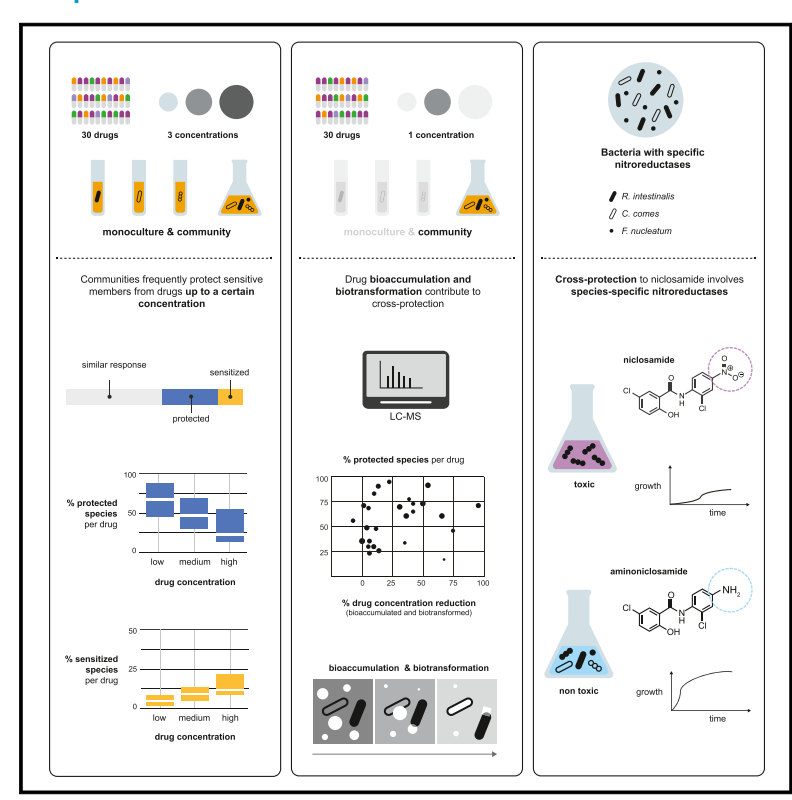


Emergence of community behaviors in the gut microbiota upon drug treatment

Graphical abstract



Highlights

- Bacteria can be protected from and sensitized to drugs in a community context
- Cross-protection and community resilience dissipate at high drug concentrations
- Drug biotransformation and bioaccumulation can partially explain communal protection
- Enzyme specificity and expression dictate detoxification of nitroaromatic drugs

Authors

Sarela Garcia-Santamarina, Michael Kuhn, Saravanan Devendran, ..., Michael Zimmermann, Peer Bork, Athanasios Typas

Correspondence

kp533@mrc-tox.cam.ac.uk (K.R.P.), michael.zimmermann@embl.de (M.Z.), bork@embl.de (P.B.), typas@embl.de (A.T.)

In brief

A comparison of the effects of pharmaceuticals on different gut bacterial species when grown alone or as part of a community shows that complex microbial communities can protect, and less frequently sensitize, community members to the treatment. Both drug biotransformation and bioaccumulation are key to community protection, which can be overwhelmed at high drug concentrations.









Article

Emergence of community behaviors in the gut microbiota upon drug treatment

Sarela Garcia-Santamarina,^{1,2,5,10} Michael Kuhn,^{2,10} Saravanan Devendran,² Lisa Maier,^{1,6,7} Marja Driessen,² André Mateus,^{1,8} Eleonora Mastrorilli,² Ana Rita Brochado,^{1,6,7} Mikhail M. Savitski,¹ Kiran R. Patil,^{2,9,*} Michael Zimmermann,^{2,*} Peer Bork,^{2,3,4,*} and Athanasios Typas^{1,2,11,*}

- ¹European Molecular Biology Laboratory, Genome Biology, Heidelberg, Germany
- ²European Molecular Biology Laboratory, Structural and Computational Biology, Heidelberg, Germany
- ³Max Delbrück Center for Molecular Medicine, Berlin, Germany
- ⁴Department of Bioinformatics, Biocenter, University of Würzburg, Würzburg, Germany
- ⁵Present address: Instituto de Tecnologia Quimica e Biologica, Universidade Nova de Lisboa, Oeiras, Portugal
- ⁶Present address: Interfaculty Institute of Microbiology and Infection Medicine, University of Tübingen, Tübingen, Germany
- ⁷Present address: Cluster of Excellence "Controlling Microbes to Fight Infections", University of Tübingen, Tübingen, Germany
- ⁸Present address: Department of Chemistry, Umeå University, Umeå, Sweden
- ⁹Present address: The Medical Research Council Toxicology Unit, University of Cambridge, Cambridge, UK
- ¹⁰These authors contributed equally
- ¹¹Lead contact

*Correspondence: kp533@mrc-tox.cam.ac.uk (K.R.P.), michael.zimmermann@embl.de (M.Z.), bork@embl.de (P.B.), typas@embl.de (A.T.) https://doi.org/10.1016/j.cell.2024.08.037

SUMMARY

Pharmaceuticals can directly inhibit the growth of gut bacteria, but the degree to which such interactions manifest in complex community settings is an open question. Here, we compared the effects of 30 drugs on a 32-species synthetic community with their effects on each community member in isolation. While most individual drug-species interactions remained the same in the community context, communal behaviors emerged in 26% of all tested cases. Cross-protection during which drug-sensitive species were protected in community was 6 times more frequent than cross-sensitization, the converse phenomenon. Cross-protection decreased and cross-sensitization increased at higher drug concentrations, suggesting that the resilience of microbial communities can collapse when perturbations get stronger. By metabolically profiling drug-treated communities, we showed that both drug biotransformation and bioaccumulation contribute mechanistically to communal protection. As a proof of principle, we molecularly dissected a prominent case: species expressing specific nitroreductases degraded niclosamide, thereby protecting both themselves and sensitive community members.

INTRODUCTION

Commonly prescribed therapeutics are associated with changes in the composition and function of the human gut microbiome. ^{1,2} Hundreds of drugs, including both antibiotics and those targeting human proteins, can directly inhibit the growth of commensal gut bacteria at physiologically relevant concentrations. ^{3,4} Reciprocally, drug sequestration or metabolization by gut bacteria can affect the bioavailability, efficacy, mode of action, and adverse effects of pharmaceuticals, thereby contributing to the interpersonal variability of drug responses. ^{1,5} Further molecular understanding of such drug-gut microbe interactions is crucial to designing improved therapies with fewer side effects, including dysbiosis.

Several studies have used *in vitro*, *ex vivo*, and *in vivo* approaches to probe the impact of a limited set of drugs in diverse communities, showing both that drugs affect the community

biomass and structure 6-10 and that communities affect drug activity via mechanisms that include drug biotransformation 5,7,11-13 and bioaccumulation. Yet it remains unclear whether and to what extent such drug-microbial interactions in communities reflect the composite of effects observed in monocultures and/or whether communal behaviors can mask or augment the single drug-microbe interactions. This understanding is crucial for our ability to predict the responses of complex communities to drug treatment and to dissect drug-microbiota interactions based on simpler and more controlled *in vitro* experimental setups.

Here, we assembled a synthetic community containing 32 representative species of the healthy human gut microbiota³ and compared the effect of 30 diverse drugs on 21 species reproducibly detected in the community versus in isolation. We detected at least one species being protected or sensitized in the community setting for all drugs tested, and in total, a quarter







of all drug-microbe interactions (465/1,823 cases; see STAR Methods) changed in the community setting. Cross-protection was the most frequent scenario, indicating that communities are more resilient to external insults than individual bacteria. However, such communal protective strategies decreased with increasing drug concentrations, while cases of cross-sensitization increased. Thus, at higher drug concentrations, communities are disturbed the most-not only because more species may be targeted by the drug but also because communities lose capacity for cross-protection and negative interactions (cross-sensitization) increase. Moreover, we demonstrated that both drug biotransformation and drug bioaccumulation contributed to many cross-protection instances and mechanistically dissected a case of communal protection, identifying the species protecting the community and the enzymes degrading the drug. Using knowledge about detoxifying species, we could design synthetic communities that would enable growth of otherwise highly sensitive communities, opening the path for future use of such knowledge to optimize community composition to reduce adverse drug effects or increase drug efficacy. Overall, we provide insights into the degree of emerging behaviors upon treatment of microbial communities with drugs, identify some of their underlying mechanisms, and map their dependence on drug concentration.

RESULTS

Evaluating the impact of drugs on the composition of a complex synthetic community

We assembled a synthetic community of 32 species from 26 genera across 6 phyla (Table S1), cultured at 37°C under anaerobic conditions in Gifu Anaerobic Medium Broth, Modified (mGAM). We selected mostly type strains of these prevalent and abundant human gut species, as they are broadly available and used. Overall, we used most of the 38 species previously selected to be representative of the healthy human gut microbiome and tested for their interactions with over 1,200 drugs,3 and six species were omitted because we could not differentiate them robustly from existing members by 16S sequencing. Combined, the 32 species accounted for 63% and 41% of the median assignable relative abundance at the genus level in fecal samples from the Human Microbiome Project¹⁴ (HMP, N = 237) and from MetaHIT¹⁵ (N = 665, Figure S1A), respectively. From over 1,200 drugs previously tested against gut microbes in isolation,3 we selected 30 representative drugs that inhibited the growth of a variety of species and spanned therapeutic areas (Figure S1B; Table S1). Out of the 30 tested drugs, 21 were human-targeted and 9 were anti-infective drugs (Figure S1B; Table S1). Drug concentrations were selected to always include 20 μM, as previously screened,³ and two additional concentrations, adjusted to the drug activity and colon concentrations (Figure S1B; Table S1). In most cases, concentrations were varied by multiples of 4 (e.g., 5, 20, and 80 µM). For fifteen of the human-targeted drugs, at least one of the tested concentrations fell within 3-fold of the estimated colon concentrations (Figure S1B; Table S1). By contrast, antibiotics were tested in concentrations below those estimated to be present in the colon, since at such high concentrations many commensals were inhibited and the community barely grew in vitro.

To probe the effect of a drug on the community, we added the drug when combining the individual species that formed the community (Figure 1A). We passaged the community (1:50 dilution) once after growing it 24 h into medium containing the respective drug and grew it for another 24 h. At the end of the second passage, relative species abundance was determined by 16S amplicon sequencing. We found high correlations between the three biological replicates (median Spearman correlation between relative abundances $r_s = 0.91$ for controls and $r_s = 0.88$ for drug treatment; Figure S1C) and between the two technical replicates performed for each biological replicate (median $r_s = 0.96$ for controls and $r_s = 0.97$ for drug treatment; Figure S1C). To assess the impact of drug treatment on each species in the community, we normalized species abundances, using the community's final optical density (OD, set to 1 for controls) as a proxy for total cell number (Figure 1B). As this normalization method is an approximation, we confirmed that the main findings of this study also held when relative species abundances were directly used (Figures S1D and S1E; see STAR Methods). To determine the effect of drug treatment, we used the ratio of the species abundance between treatment conditions and untreated controls (Figure 1C). Eleven species were below the level of detection in untreated controls, and therefore we excluded them from further analysis. Those eleven species included some, but not all, of the slower-growing species in mGAM (Figure S1F). Interestingly, 7 of these low-abundance species could be detected in at least one treatment condition (Table S1), suggesting that drugs can open niches for otherwise less fit community members, for example, by removing competitors for same niche or slowing down the growth of otherwise rapidly growing species. Twenty of the 21 species that remained above detection level in community after passaging in vitro were also recently found to stably colonize germ-free mice as community and provide colonization resistance against pathogens. 16

Community behaviors emerge during drug treatment

All 21 species kept for further analysis were also treated individually with the 30 drugs (at 3 concentrations), and their growth was monitored (Figures 1D and 1E; Table S1). We calculated the area under the growth curve (AUC) and normalized it for the vehicle (DMSO)-treated controls (STAR Methods). For a total of 1,823 drug-species combinations, we compared the response to the drug in community and in monoculture. From the 1,890 possible drug-species combinations (21 species × 30 drugs × 3 concentrations), we excluded 4 cases in which growth data in monocultures were not reproducible and the highest concentration for 3 drugs (chlorpromazine, ciprofloxacin, and doxycycline) in which the community did not grow at all. Three outcomes were identified (Figures 1C, 1E, 2A, and 2B, using methotrexate as an example): (1) expected outcome - growth was similarly affected (Veillonela parvula) or unaffected (Escherichia coli) in both community and monoculture; (2) cross-sensitization (emergent communal behavior)-the species growth was not affected by the drug when alone, but its abundance was reduced in the community (Fusobacterium nucleatum); (3) cross-protection (emergent communal behavior)—the species was inhibited in



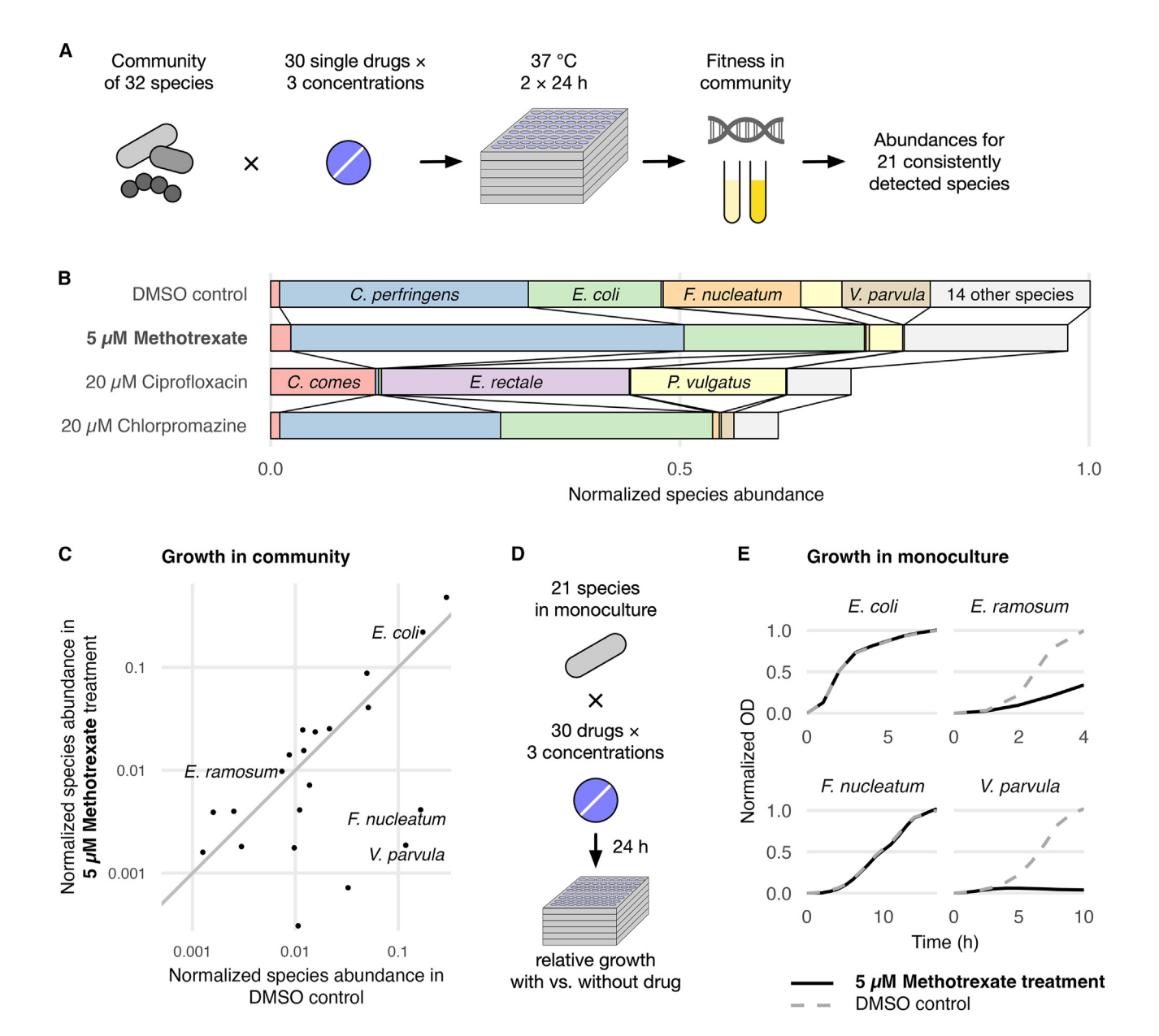


Figure 1. Measuring drug impact on gut bacteria in community and in isolation

(A) A community of 32 gut bacterial species was treated with 30 drugs in 3 concentrations. The community was treated with drug upon assembly for 48 h, with an intermediate passage step (1:50 dilution) at 24 h. Community growth was measured by following OD and relative species abundance by 16S rDNA amplicon sequencing at 48 h. Twenty-one species were reproducibly detected in vehicle (DMSO control) and used thereafter.

- (B) Examples of normalized species abundances in vehicle (DMSO control) and in three selected drugs and concentrations in the community. The abundance for each species of the community is normalized by the final OD of the community.
- (C) Example of the effect of 5 μ M methotrexate in the community, comparing species normalized abundances between DMSO control and treated conditions. Species along the identity line were not influenced by the drug, while species below were inhibited in the presence of methotrexate.
- (D) The 21 species reproducibly detected in the community were also tested in the same panel of drugs as in (A) in isolation. Fitness was calculated by comparing the growth with versus without drug.
- (E) Examples of the effect of 5 μM methotrexate on selected species in monoculture compared with DMSO controls. While *E. coli* and *V. parvula* behaved the same in community (C) and isolation (E), *E. ramosum* and *F. nucleatum* were only inhibited in isolation (E) and in the community (C), respectively. See also Figure S1.

monoculture but grew normally in community (*Erysipelatoclostri-dium ramosum*). To assess the degree of cross-protection and cross-sensitization per drug, we calculated the percentage of

species that were either protected or sensitized in the community. For protection, we divided by the total number of species that the drug inhibited in monoculture (as only those could be



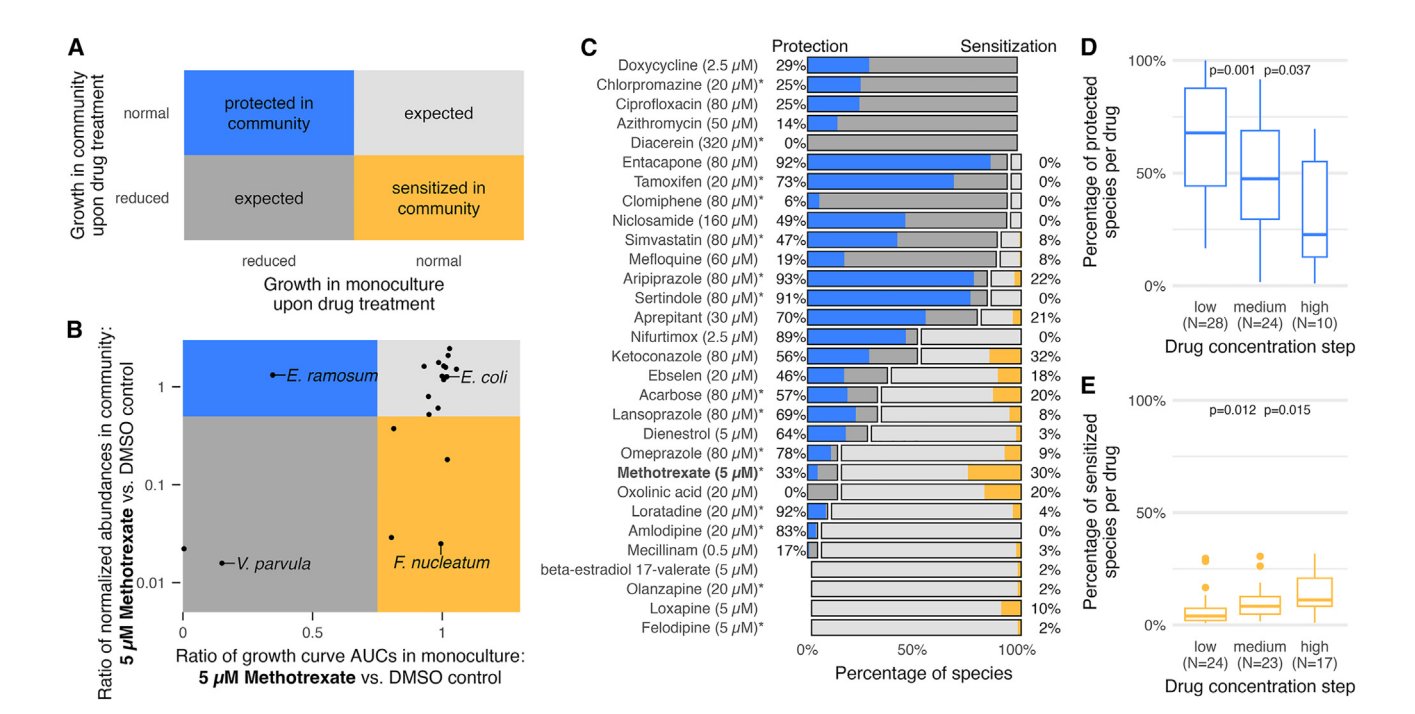


Figure 2. Emergent community behaviors are common upon drug treatment

(A) Comparing species growth in monoculture and in community in response to drug treatment. "Expected" refers to similar growth in both community and monoculture (light and dark gray areas), "protected in community" refers to species that are inhibited by the drug in monoculture but remain relatively unperturbed in the community (blue area), and "sensitized in community" refers to species being unaffected in monoculture but inhibited by the drug in the community (vellow area).

(B) Examples of community-emergent behaviors for 5 μM methotrexate treatment. *E. coli* growth was unperturbed both in monoculture and in the community (expected), *V. parvula* was inhibited in both cases (expected), *E. ramosum* was only inhibited in monoculture (protected in community), and *F. nucleatum* growth was only reduced in the community setting (sensitized in community).

(C) Percentage of the 21 species across replicates that show expected or emergent behaviors (protection or sensitization in community) in all drugs tested at the concentration closest to the estimated colon concentration, or at 20 µM for those cases that the colon concentration could not be estimated (Figure S1B). The asterisk denotes drug concentrations that are within a factor of three of the estimated intestinal concentration.

(D and E) Higher drug concentrations bypass community resilience. A median of 68% sensitive species in 28 drugs was protected in the community at the lowest drug concentrations, but this significantly decreased to 47% (in 24 drugs) at the intermediate concentration and to 23% (in 10 drugs) at the highest concentration (D). For drugs with resistant species (24 drugs) at the lowest concentrations, sensitization occurred for a median of 4% of resistant species, and this increased to 8% (in 23 drugs) and 11% (in 17 drugs) at the intermediate and high concentrations, respectively (E). p values were calculated using paired Wilcoxon signed-rank tests. The boxplots represent the distribution of the data. The line within the box represents the median, and the lower and upper hinges correspond to the 25th and 75th percentiles, respectively. The distance between the 25th and 75th percentiles is the inter-quartile range (IQR). The lower and upper whiskers extend to the smallest and lowest values up to 1.5 * IQR from the hinge, respectively. Data points beyond the whiskers are outliers, individually plotted.

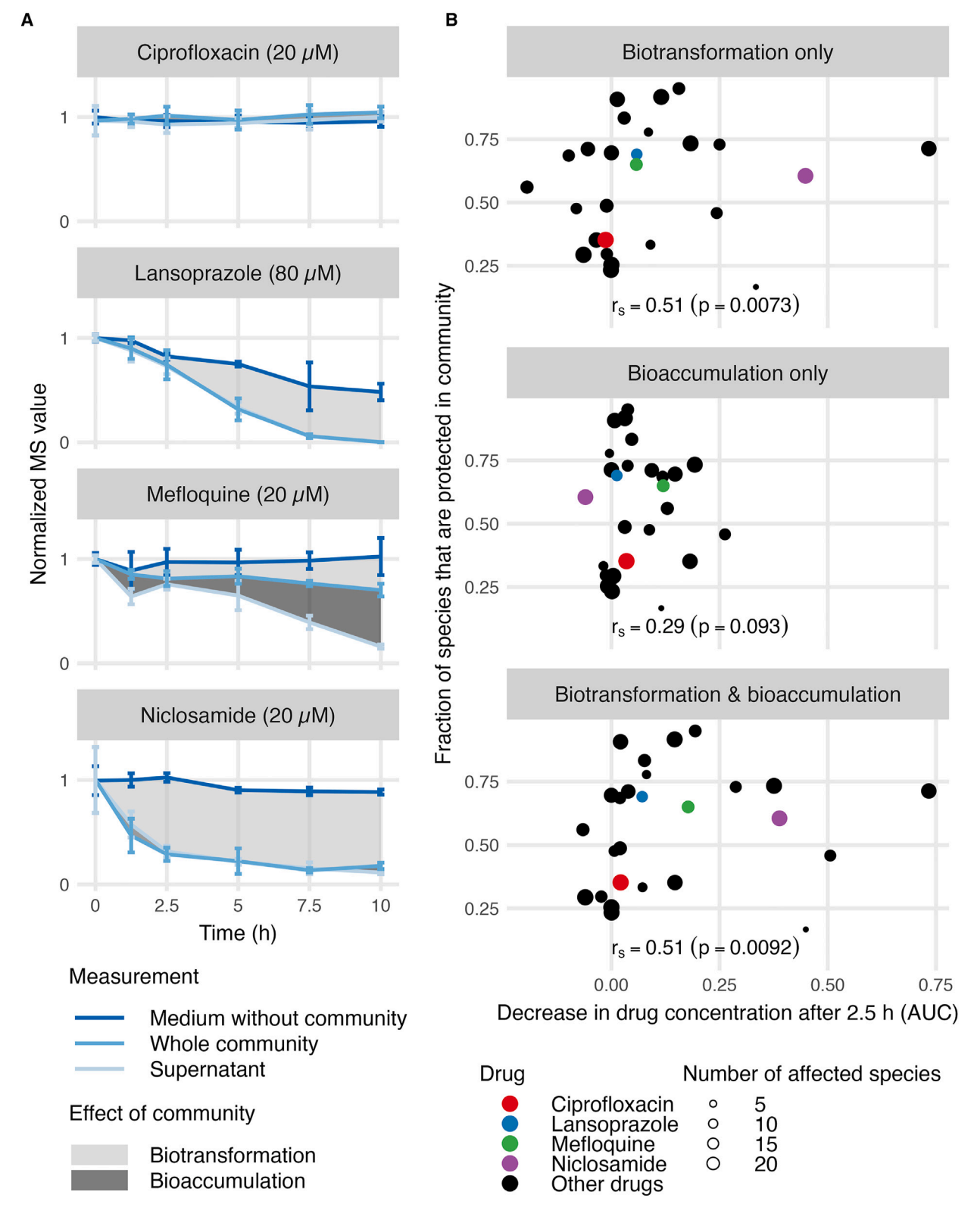
See also Figures S2 and S3.

protected in community), whereas for sensitization, we divided by the total number of species that grew normally in single-species experiments (Figure 2C, for the treatment amount closest to the gut concentration; Figure S2 for all treatment conditions). We observed at least one emergent behavior for all drugs probed, and in total 26% of drug-microbe interactions changed in the community setting. When taking into account only drug-sensitive species, protection in the community amounted to 47% of all cases, whereas community-specific sensitization was observed in 8% of all cases of resistant species. At the drug concentrations closest to the estimated human gut concentrations, these fractions were very similar with 49% and 9%, respectively. Overall, this suggests that numerous community-dependent protection and sensitization events can be expected upon drug treatment of human gut microbiotas, and those can vary between individuals as they harbor different community compositions.

High drug concentrations overwhelm community resilience

For each drug, we tested 3 concentrations. When starting from concentrations at which there was at least one sensitive species in monoculture (to be able to detect cross-protection), we could detect a significant drop in the percentage of protected species within the community across all drugs as the drug concentration increased (Figure 2D). Vice versa, the percentage of sensitized species significantly increased at higher drug concentrations (Figure 2E). Since the concentration steps were not always equally spaced, we also verified the concentration dependence in a separate model that uses the actual drug concentrations (Figures S3A and S3B). Overall, this means that the community stays relatively unaffected at low drug concentrations since the perturbation is buffered and sensitive species are protected. By contrast, the impact on composition





(legend on next page)





increases disproportionally at higher drug concentrations, as not only does the community fail to protect other members, but negative interactions emerge that sensitize otherwise resistant species.

Bacterial drug biotransformation and bioaccumulation underpin emergent cross-protection

Many mechanisms could be driving the prevalent emergent behaviors we observed: interspecies interactions, new niches created by reduced growth of some species, altered stress responses and/or triggering of toxic molecule secretion, 17-19 and/or modifications in the drug availability and structure. Since previous work had showcased the extended ability of gut microbes to transform or intracellularly accumulate drugs, 5,11,12 we decided to assess the degree to which emergent communal phenotypes, and especially cross-protection, could be explained by such phenomena. To this aim, we measured drug concentrations over time using liquid chromatography-coupled mass spectrometry (LC-MS) in the same synthetic community upon treatment with the same panel of drugs as above, typically at the concentration for which we observed the highest percentage of emergent behaviors (Figure S2). Samples were collected on the second day of treatment at different time points after passage into fresh, drug-exposed medium (0, 1.25, 2.5, 5, 7.5, and 10 h after treatment). We collected two fractions per community: one containing the whole community (WC), i.e., both supernatant (SN) and bacteria, and one containing only SN, to be able to distinguish between biotransformation and bioaccumulation.5 In parallel, we used only mGAM and the same time course to assess drug decay in the medium. For each time course, we normalized concentrations to the maximum value among the two first time points of the time course and calculated AUCs. Overall, biological replicates were consistent, with mean standard deviation between replicates for all measurements being 8% for both community experiments and media control. From the time courses of each drug, we used AUCs to calculate the extent of biotransformation (media control minus WC), bioaccumulation (WC minus SN), and both phenomena (media control minus SN) (Figures 3A and S4A; Table S2). For example, the antibiotic ciprofloxacin was stable across all conditions; the proton-pump inhibitor lansoprazole decayed on its own, and this process was accelerated by the community; the antiparasitic niclosamide was rapidly metabolized by the community; and the antimalaria drug mefloquine was both bioaccumulated and biotransformed (Figure 3A).

We found an overall positive correlation between the fraction of species that were protected by the community and the degree

to which the drug was biotransformed by the community (Figure 3B), with the two earliest time points (1.25 and 2.5 h) showing significant correlations (Figures 3B and S4B). By contrast, bioaccumulation only mildly correlated with the fraction of both protected and sensitized species at early time points, with only the first time point showing a significant correlation with protection (Figures 3B, S4B, and S4C). When combined with biotransformation, bioaccumulation often increased the overall correlation with the fraction of protected species in the community (Figures 3B, S4B, and S4C). Overall, this means that the protective community effects can be at least partially explained by the drug being transformed (and to some degree accumulated) by one or more species in the community. Nonetheless, there are other mechanisms at play that remain to be elucidated in the future; for example, dienestrol was neither biotransformed nor bioaccumulated, yet 49% of susceptible species were protected in the community. In such cases, altered metabolism of drugtreated species may create new niches or neutralize the drug effect for the sensitive species. In contrast to communal protection, cross-sensitization did not correlate with biotransformation and only partially correlated with bioaccumulation (Figures S4B and S4D). This could be due to the smaller number of cases identified. Having a better understanding of what drives cross-protection, we decided to study some of the underlying mechanisms in further detail.

Different species protect against different nitroaromatic drugs in communities

All three nitroaromatic drugs used in the screen, the antiparasitic drugs niclosamide and nifurtimox, and a drug to treat Parkinson's disease, entacapone, were rapidly biotransformed by the community (Figure S4A). At the highest tested concentration, these drugs inhibited on average 92% of the tested species in monoculture (Table S1). In line with the observed biotransformation, we found 47% of these sensitive species to be protected by the community (Figure S2). Since both activation and detoxification of nitroaromatic compounds rely on reduction of the nitro group, ^{20,21} we wondered whether it is the same set of microbes with potent nitroreductases that efficiently transformed the drugs to an inactive form.

To explore this further, we selected seven species from the community, which covered a wide range of sensitivities to niclosamide in monoculture (Figure 4A). Using LC-MS, we checked for the ability of these seven species to reduce niclosamide to its amine form. Three out of the four (partially) resistant species in monoculture (Roseburia intestinalis, Coprococcus comes, and F. nucleatum; Figure 4A) stoichiometrically and rapidly

Figure 3. Bacterial drug biotransformation and bioaccumulation drive community cross-protection

(A) Representative examples of community effects on drug biotransformation and bioaccumulation during a 10 h treatment. Drug concentrations were measured by LC-MS in the 32-species synthetic community for 27 drugs (Figure S4A). For each time course, we normalized concentrations to the start of the time course (using time point with the highest raw measurement at 0 or 1.25 h) and calculated the mean drug concentration per time point. Bioaccumulation can be calculated by comparing the drug remaining in whole community and in supernatant (dark gray), and biotransformation by comparing the drug alone with the drug remaining whole community (light gray). Ciprofloxacin was stable in the community, lansoprazole was unstable in mGAM and decayed further in the community, mefloquine was biotransformed and bioaccumulated, and niclosamide was rapidly biotransformed by the community. The error bars represent the standard deviation of the replicates.

(B) Fraction of protected strains correlated with degree of drug biotransformation and bioaccumulation by the community. p values were calculated by permutation tests using 100,000 samples.

See also Figure S4.



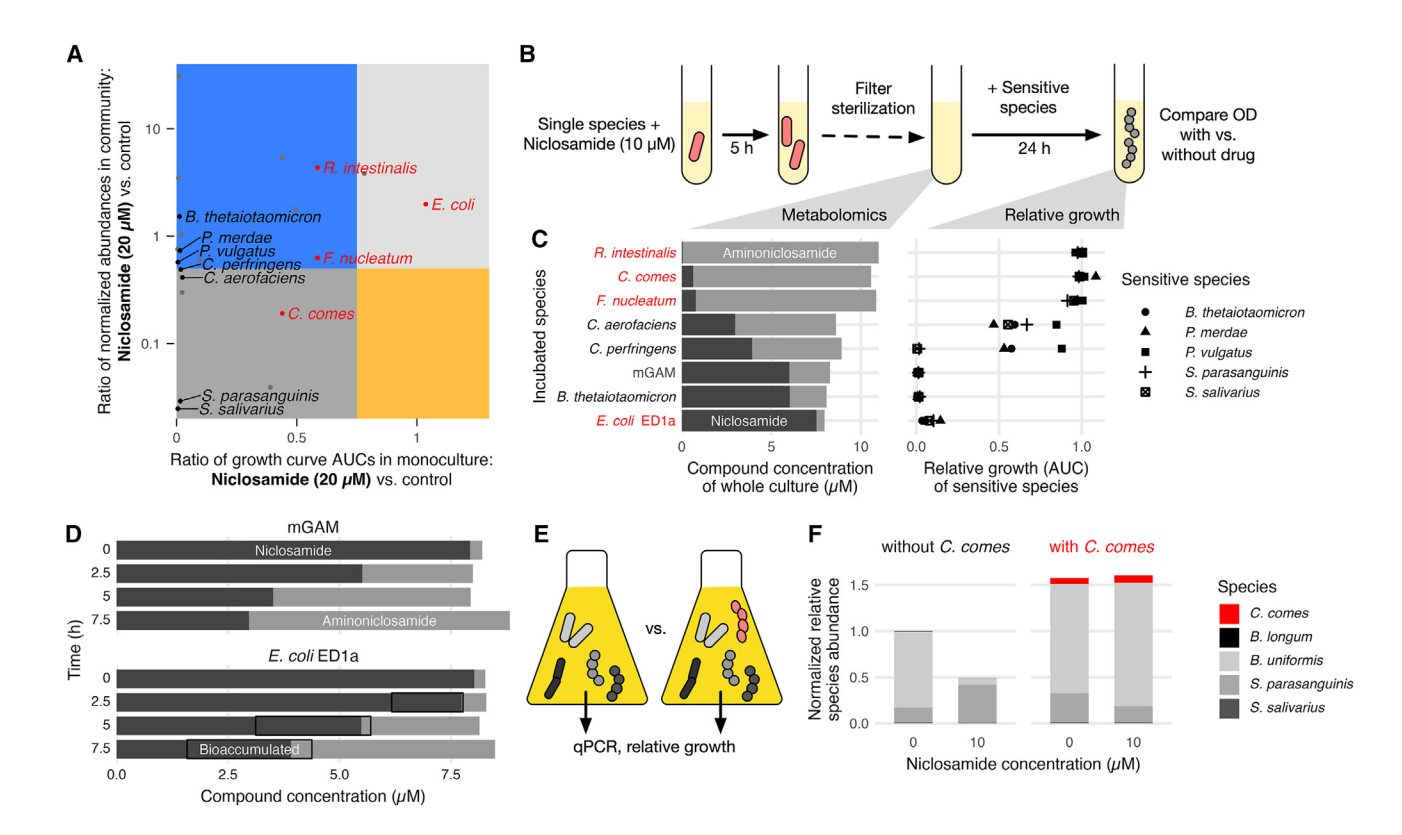


Figure 4. Specific species protect the community from niclosamide

(A) Community-emergent phenotypes in $20~\mu M$ niclosamide. Representation of species that grow in community as expected from monoculture (gray areas) that are cross-protected (blue area) or cross-sensitized (yellow area) in the community. Species used in further tests are highlighted: partially/full resistant species to niclosamide in red and sensitive species in black.

(B) Experimental strategy used to disentangle contributions of individual species to community protection from niclosamide. Species were incubated with niclosamide for 5 h, after which cultures were analyzed by targeted metabolomics to quantify niclosamide and aminoniclosamide (see also Figures S5A and S5B). In separate experiments, the same species were treated with vehicle (DMSO control) or 10 μM niclosamide for 5 h, after which cultures were filter-sterilized. Spent media from these cultures was mixed 1:1 with fresh mGAM and used to grow other niclosamide-sensitive species. Growth of these other species in spent media from drug-treated cultures was normalized to their growth in spent media from DMSO cultures (controls).

(C) Left, following the scheme in (B), quantification of niclosamide and aminoniclosamide in culture media of the indicated species (text color as in A) after 5 h incubation with niclosamide. Right, relative growth of the indicated species (sensitive to niclosamide; see A) in spent media from the niclosamide-treated cultures. (D) Quantification of niclosamide and aminoniclosamide concentrations in medium control (upper) and in cultures of *E. coli* ED1a cells after treatment with 10 μM niclosamide for the indicated times (lower). Boxes denote the amount of bioaccumulated drug in *E. coli* ED1a. To determine them, we subtracted the measured compound concentrations in supernatants from those measured in whole-cell cultures. Niclosamide is more stable (i.e., less reduced to aminoniclosamide) in *E. coli* ED1a cell cultures (lower) than in the medium control (upper) because it is bioaccumulated in ED1a cells (see also Figure S5C).

(E and F) Addition of a niclosamide-detoxifying species can rescue a synthetic community from niclosamide treatment. *C. comes* restores growth of a niclosamide-treated community, yielding species abundances similar to that of the untreated control (see also Figure S6F). In addition to drug protection, *C. comes* promotes the overall community growth via unknown mechanisms.

See also Figure S5 and S6.

reduced niclosamide to aminoniclosamide (Figures 4B, 4C, S5, and S6A), which was not toxic to any of the gut bacterial isolates tested (Figure S6B). Indeed, this biotransformation of the drug to the inactive amino form resulted in protection of niclosamidesensitive species from niclosamide toxicity, as we showed by growing sensitive species in spent media of bacteria with biotransformation capacity (Figure 4B). The degree of protection of sensitive species was directly related to the ability of the protecting species to degrade the drug (Figure 4C; Table S2).

In contrast to the other three (partially) resistant species, we found that the most resistant species, *E. coli* ED1a, could not degrade niclosamide, and the drug was even more stable in the culture than in the medium control (Figures 4C and S5C;

Table S2). We hypothesized that *E. coli* ED1A bioaccumulates niclosamide, preventing the non-enzymatic reduction of the drug²² in the medium. Indeed, by using drug-treated cultures and spent media, we showed that a significant amount of niclosamide bioaccumulated in *E. coli* ED1a (\sim 2 μ M in 5 h, Figure 4D; Table S2) without affecting the fitness of the organism. However, this amount of bioaccumulation in *E. coli* ED1a allowed only limited protection of other sensitive species in the spent media (Figure 4C; Table S2), as the niclosamide remaining in the media was mostly above to the minimal inhibitory concentrations (MICs) of the sensitive species (Figure S6C).

In stark contrast to its inability to reduce niclosamide, *E. coli* ED1a had high protective capacity for nifurtimox, completely

Cell Article



transforming 20 μ M nifurtimox in 5 h and fully protecting nifurtimox-sensitive species (Figures S6D and S6E). Another fully resistant species to nifurtimox, *Streptococcus parasanguinis* (Figure S6D), only partially metabolized the drug after 7.5 h incubation and hence offered limited protection to sensitive species (Figure S6E; Table S2). Overall, this highlights the diversity of drug-microbe interaction mechanisms, even with drugs with the same functional group that are subject to the same type of bacterial transformation. It also highlights that the degree of resistance is not predictive of the ability to protect other species in the community, as resistance mechanisms differ.

We further wondered whether we could use this knowledge of selective protection to engineer communities that are more robust to drug treatment. To do this, we grew a small community of gut bacteria sensitive to niclosamide, composed of $Bifidobacterium\ longum$, $Bacteroides\ uniformis$, S. parasanguinis, and S. salivarius (MIC $\leq 1.25\ \mu M$), to which we added or not the detoxifier C. comes (Figure 4E). C. comes partially restored the growth of the community, even after 10 μM niclosamide treatment, yielding species relative abundances similar to those of the untreated control (Figures 4F and S6F). C. comes provided communal resistance to niclosamide, despite itself only growing modestly in the community, highlighting that protection can also be offered from members that are less abundant in the community.

Nitroreductase expression and specificity determine ability to reduce nitroaromatics

To pinpoint the mechanism by which niclosamide cross-protection occurred, we looked for the nitroreductases encoded in the genomes of the protecting and sensitive species. Oxygen-insensitive or type I pyridine nucleotide-flavin mononucleotide (NAD(P)H/FMN)-dependent nitroreductases reduce nitroaromatics through stepwise additions of two electrons to nitroso-, hydroxylamino-, or amino-aromatics.²³ FMNdependent nitroreductases constitute a large and diverse family of proteins, mainly present in bacteria, which have been recently reclassified into 14 subgroups according to their sequence similarities.²⁴ We found that all species in our community encode at least two of these enzymes belonging to different subgroups (Table S3). To further understand the basis of niclosamide reduction, we focused on two species: (1) R. intestinalis, moderately resistant to niclosamide and a good protector, encoding only two putative FMN-dependent nitroreductases (other resistant species encoded more nitroreductases), and (2) P. vulgatus, sensitive to niclosamide (MIC = 0.625 μM), but intriguingly encoding seven putative nitroreductases (Table S3). To test the ability of each of these nitroreductases to degrade niclosamide, we cloned and overexpressed them in the sensitive P. vulgatus. Overexpressing any of the two R. intestinalis nitroreductases conferred an 8-fold or more increase in MIC to niclosamide for P. vulgatus (Figures 5A and S6G), suggesting that these enzymes are responsible for the resistance of R. intestinalis in niclosamide. Indeed, nitroreductase C7GA87 was highly expressed in R. intestinalis (Figure 5B). Interestingly, overexpression of two out of the seven P. vulgatus nitroreductases conferred also significant resistance to niclosamide (Figures 5A and S6G). We reasoned that these proteins should be silent or lowly expressed from endogenous locus, and hence *P. vulgatus* is sensitive to niclosamide. Indeed, both proteins had low abundance, which was not further induced by niclosamide in monoculture (Figure 5B). Overexpression of nitroreductase Pv2039 led to >16-fold increase in protein levels (Table S3) and 32-fold higher niclosamide resistance (Figures 5A and 5B). As expected, only *P. vulgatus* overexpressing the *R. intestinalis* nitroreductases or the endogenous Pv2039 allowed other niclosamide-sensitive strains to grow (Figures 6C and 6D).

Our results indicate that nitroreductases are specific to the substrate. When we overexpressed the same nitroreductases as the ones above in *P. vulgatus*, resistance to nifurtimox did not change (Figure S6G), which was consistent with the sensitivity of both *P. vulgatus* and *R. intestinalis* to nifurtimox (Figure S6D). Thus, many species may have the capacity to biotransform drugs, but the respective selective enzymes may not be expressed and/or induced upon drug treatment.

DISCUSSION

In recent years, advances in gut microbiota culture techniques have made it possible to systematically determine the direct interactions between hundreds of commonly used drugs and specific members of the gut microbiota. 3,6,12 However, little is known about whether these direct drug-bacterial species interactions are relevant when the same strain/species is part of a bacterial community. Here, we show that 74% of a total of 1,823 directly determined drug-species interactions remained the same in a community context. Hence, singlespecies-drug interactions are relatively good predictors of what will happen to a species when it is part of a community. This is consistent with decades of clinical work where antibiotic sensitivity of enteric pathogens is tested in isolation and not in community settings. Nevertheless, communal behaviors were substantial and were present in every drug we tested. Protection of sensitive species was the most common outcome, especially at low drug concentrations. At higher concentrations, closer to those found in the colon, community protection decreased, with more species behaving the same as when growing alone.

Based on targeted metabolomics data, we established that bacterial drug biotransformation partially explains community protection phenotypes. This implies that in most cases drug biotransformation yields harmless or less toxic products. In our in vitro setting, drug bioaccumulation only mildly correlated with protective phenotypes. This could be because we added the drug during passaging, meaning that at the beginning there is a relatively low bacterial biomass that could accumulate the drug. Since this low biomass situation is less relevant for the human gut, we may be underestimating the role of bioaccumulation with our experimental setup. Bioaccumulation has only recently been reported for drugs and gut microbes.⁵ In addition to the previously reported drugs, we found here that intestinal bacteria bioaccumulate four more drugs: ebselen, mefloquine, simvastatin, and tamoxifen. Ebselen may accumulate due to its ability to bind to thiol groups.²⁵ In the case of tamoxifen or mefloquine, bioaccumulation could stem from their ability to interact with





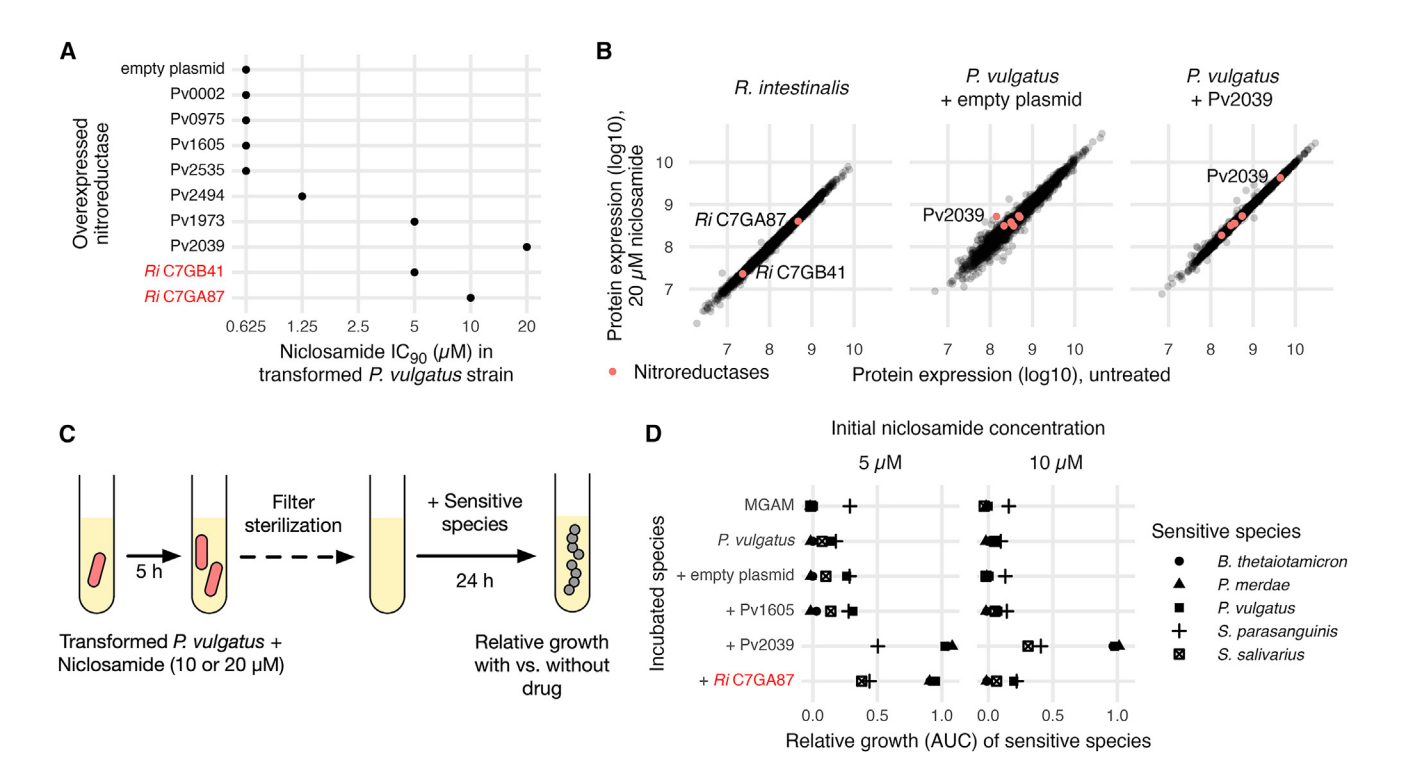


Figure 5. Specific nitroreductases protect the community from niclosamide

(A) Effect of heterologous nitroreductase overexpression on P. $vulgatus\ IC_{90}$ (μM) to niclosamide. IC_{90} represents the concentration at which 90% of the growth is inhibited (see Figure S6G for IC curves). P. vulgatus strains transformed with empty plasmid or plasmids overexpressing different P. vulgatus or R. intestinalis nitroreductases, as indicated, were treated with niclosamide, and growth was monitored by measuring the OD_{578} during 24 h.

(B) Comparison of proteome expression between niclosamide (20 μM for 30 min; y axis) and vehicle (DMSO control, x axis) treated cultures of *R. intestinalis*, *P. vulgatus* transformed with an empty plasmid, and *P. vulgatus* overexpressing the nitroreductase Pvu2039. The two putative *R. intestinalis* nitroreductases and the seven putative *P. vulgatus* nitroreductases are highlighted in red.

(C) *P. vulgatus* expressing different nitroreductases has different abilities to protect niclosamide-sensitive species. Similar to experiment in Figures 4B and 4C, *P. vulgatus* strains carrying different nitroreductases were treated with DMSO control, 10 μ M, or 20 μ M niclosamide for 5 h, after which cultures were filter-sterilized. Spent media from these cultures was mixed 1:1 with fresh mGAM and used to grow niclosamide-sensitive species.

(D) Following the scheme in (C), growth of the indicated strains in spent media from niclosamide-treated cultures. Growth of the sensitive strains in spent media of treated cultures was normalized with their growth in spent media from untreated cultures (controls). See also Figure S6.

membranes, as previously shown for *Bacillus stearothermophilus* and *E. coli*, respectively. ^{26,27} The case of simvastatin is interesting, since previous studies suggested a link between microbiome composition and the efficacy of the drug in lowering low-density lipoprotein (LDL) cholesterol in patients. ^{28–30} Statins are widely prescribed in western countries ³¹ and are hence commonly found in wastewater. ³² Due to their high water-octanol partition coefficient, statins tend to bioaccumulate in aquatic animals, causing a serious environmental problem. ^{33,34} It would interesting to investigate in the future if the bioaccumulation of statins in bacteria has implications for drug efficacy in patients and/or may also affect the accumulation of the drug in environmental reservoirs.

Our data underline the broad ability of the microbiota to transform xenobiotics. Working with a bottom-up assembled synthetic community allowed us to gain insights into the biotransformation mechanisms that lead to communal protection. We focused on nitroaromatic compounds and observed that the nitroreductases that reduce them are rather specific. For example, both nitroreductases of the niclosamide-resis-

tant *R. intestinalis* efficiently reduced niclosamide but not nifurtimox. Importantly, *P. vulgatus* encoded nitroreductases that could render it resistant to niclosamide but did not express them in relevant amounts even in the presence of the drug. This denotes that gut bacteria likely have an even larger potential to transform drugs than previously appreciated, which would render them able to evolve resistance if exposed to the drug for longer periods.

Albeit rare at low drug concentrations, cross-sensitization became more frequent as emergent behavior at higher drug concentrations. Cross-sensitization may arise from direct or indirect effects. A drug can itself become more toxic to a given species in a community setting because uptake mechanisms get activated, resistance mechanisms dampened, or the drug is transformed to a more toxic product by another species. Biotransformation to more toxic products did not occur for the drugs we tested, as biotransformation lacked any correlation to cross-sensitization (Figures S4B and S4D). On the other hand, more indirect mechanisms, such as strain competition arising from altered nutrient utilization dynamics





or the induction of toxic stress responses by other members of the community targeted by the drug, can also be at play. It has been previously reported that drug treatments can trigger virulence factor and toxin production, especially at low antibiotics doses. ^{17–19} Although the underlying mechanisms behind such cases remain to be explored, cross-sensitization further decreases the community richness. Together with the loss of cross-protection at high drug concentrations, they presumably lead to an accumulative strong impact in community stability.

In summary, we established that most drug-gut bacteria interactions remain the same in communities, but cross-protection and/or cross-sensitization of specific community members happens for almost every drug. The knowledge of such interactions that change in the community setting could help to build more accurate predictive models of community responses to drug in the future. We further showed that communities have higher resilience than individual species to certain drugs, but up to a certain concentration limit, after which communal protection drops and cross-sensitization and individualized behaviors prevail. This resilience is partially explained by bacterial drug biotransformation activities, which are facilitated by the expanded functional diversity of the community. However, this is not the only mechanism by which communities become resilient. Understanding the remaining underlying mechanisms can facilitate the targeted design of designed communities that are resilient to specific drugs, as we show here for niclosamide. Our work also contributes to expanding the notion that drug bioaccumulation is widespread among gut bacteria.5 Understanding the drivers of bioaccumulation, as well as its potential to affect drug mode of action, merits both deeper exploration. Overall, we have used a bottom-up approach to assess the degree of communal behaviors that emerge in response to drugs and to map some of the underlying mechanisms that govern interactions between drugs and gut bacteria.

Limitations of the study

The in vitro model used in this study has enabled us to systematically assess the degree to which community effects modulate bacterial responses to drugs, the mechanisms driving such emergent communal behaviors, and their relation to drug concentrations. We opted for a synthetic community consisting of 21 prevalent and abundant human gut species at the end. This reductionist approach has numerous advantages, including control of community assembly, access to all members, accumulated knowledge of type strains used, and in vivo and in vitro community stability, which are all key for starting to understand communal behaviors. However, a single synthetic community cannot capture the genetic diversity of human microbiomes within and across individuals. The relative abundances of species within communities grown in vitro cannot fully reproduce the ones found in the human gastrointestinal tract, which may cause discrepancies between in vitro observations and potential in vivo outcomes. Specific drug-species interactions observed in vitro in our study may not translate one-toone to in vivo due to factors, such as different community composition, strain diversity, host environment, nutrition, and drug bioavailability in the colon. Hence, the specific drug interactions we report here have limited utility for clinical applications without further validation. To establish such clinical relevance, different study designs that focus on specific drugs and measure drug pharmacokinetics and drug concentrations in colon, as well as assess the impact of the drug in large number of strains and communities (to account for interpersonal variation) will be needed in the future. The study design (30 drugs covering 20 different therapeutic classes) also precludes general statements about the behaviors of specific drug classes or the identification of links between drug chemistry and microbial responses. As communal interactions to drugs seem pervasive across drug classes, future studies that focus on specific therapeutic classes and increase the number of drugs tested and strain/community variability will give power to start building associations (and hypotheses) between drug chemistry and molecular functions.

RESOURCE AVAILABILITY

Lead contact

Further information and requests for resources and reagents should be directed to and will be fulfilled by the lead contact, Athanasios Typas (typas@embl.de).

Materials availability

All plasmids and strains generated in this work are available upon request.

Data and code availability

Data are available from https://github.com/grp-bork/drugbug_Santamarina_2023.

- Raw 16S amplicon sequencing data have been deposited at the European Nucleotide Archive (ENA) under accession number ENA:
 PRJEB46619 https://www.ebi.ac.uk/ena/browser/view/PRJEB63118.
- LC-MS data from the community experiments has been submitted to the MetaboLights database under accession number Metabolights: MTBLS10112.

Code is available at https://github.com/grp-bork/drugbug_Santamarina_2023

Any additional information required to reanalyze the data reported in this
paper is available from the lead contact upon request.

ACKNOWLEDGMENTS

We thank Justin Sonnenburg and Carlos G.P. Voogdt for plasmids; Jacob Bobonis for providing the *E. coli* conjugation donor; Ece Kartal for help with primers design for qPCR; the EMBL Gene Core Facility for services and experimental assistance; Thomas Sebastian B. Schmidt and Georg Zeller for analysis and feedback of pilot experiments; Pascale Cossart and Carlos G.P. Voogdt for feedback on the manuscript; and Luis Morgado, Joel Arruda, and the ITQB Communication Office for graphical abstract design. We acknowledge EMBL, ERC grant uCARE (ID 819454), and the H-2020 Twinning project: SymbNET Genomics & Metabolomics in a Host-Microbe Symbiosis Network (grant: 952537) for funding. S.G.-S. and L.M. were supported by the EMBL Interdisciplinary Postdoc programme under the Marie Sklodowska Curie Actions COFUND (grant numbers 664726 and 291772, respectively).

AUTHOR CONTRIBUTIONS

This study was conceived by K.R.P., P.B., and A.T. and was designed by S.G.-S., M.K., L.M., M.Z., and A.T. M.K. pre-processed, curated, analyzed,





and/or contributed to the analysis of all experimental data. S.G.-S., L.M., and M.D. performed community experiments; S.G.-S. and A.R.B. performed high-throughput DNA extraction; S.G.-S., S.D., and E.M. performed metabolomics experiments and analyzed metabolomics data; S.G.-S. and A.M. performed proteomics experiments and analyzed proteomics data; S.G.-S. performed niclosamide and nifurtimox experiments; and M.M.S., M.Z., and A.T. supervised experimental work. Data interpretation was performed by S.G.-S., M.K., K.R.P., M.Z., P.B., and A.T. S.G.-S., M.K., and A.T. wrote the manuscript with feedback from all authors. M.K. and S.G.-S. designed the figures with input from K.R.P., M.Z., P.B., and A.T.

DECLARATION OF INTERESTS

The authors declare no competing interests.

STAR*METHODS

Detailed methods are provided in the online version of this paper and include the following:

- KEY RESOURCES TABLE
- EXPERIMENTAL MODEL
 - Bacterial species and growth conditions
- METHOD DETAILS
 - Chemical screening of a bottom-up assembled bacterial community of 32 species
 - O Chemical screening of bacterial monocultures
 - Quantification of community effects
 - o Spent media experiments
 - o Small community growth rescue by a drug detoxifier
 - Overexpression of nitroreductases
 - O Calculation of species abundances in human microbiomes

SUPPLEMENTAL INFORMATION

Supplemental information can be found online at https://doi.org/10.1016/j.cell. 2024.08.037.

Received: June 14, 2023 Revised: June 26, 2024 Accepted: August 20, 2024 Published: September 24, 2024

REFERENCES

- Zimmermann, M., Patil, K.R., Typas, A., and Maier, L. (2021). Towards a mechanistic understanding of reciprocal drug-microbiome interactions. Mol. Syst. Biol. 17, e10116. https://doi.org/10.15252/MSB.202010116.
- Maier, L., and Typas, A. (2017). Systematically investigating the impact of medication on the gut microbiome. Curr. Opin. Microbiol. 39, 128–135. https://doi.org/10.1016/J.MIB.2017.11.001.
- Maier, L., Pruteanu, M., Kuhn, M., Zeller, G., Telzerow, A., Anderson, E.E., Brochado, A.R., Fernandez, K.C., Dose, H., Mori, H., et al. (2018). Extensive impact of non-antibiotic drugs on human gut bacteria. Nature 555, 623–628. https://doi.org/10.1038/nature25979.
- Maier, L., Goemans, C.V., Wirbel, J., Kuhn, M., Eberl, C., Pruteanu, M., Müller, P., Garcia-Santamarina, S., Cacace, E., Zhang, B., et al. (2021). Unravelling the collateral damage of antibiotics on gut bacteria. Nature 599, 120–124. https://doi.org/10.1038/s41586-021-03986-2.
- Klünemann, M., Andrejev, S., Blasche, S., Mateus, A., Phapale, P., Devendran, S., Vappiani, J., Simon, B., Scott, T.A., Kafkia, E., et al. (2021). Bioaccumulation of therapeutic drugs by human gut bacteria. Nature 7877, 533–538. https://doi.org/10.1038/s41586-021-03891-8.
- Li, L., Ning, Z., Zhang, X., Mayne, J., Cheng, K., Stintzi, A., and Figeys, D. (2020). RapidAlM: a culture- and metaproteomics-based rapid assay of individual microbiome responses to drugs. Microbiome 8, 33. https://doi. org/10.1186/S40168-020-00806-Z.

- Van De Steeg, E., Schuren, F.H.J., Obach, R.S., Van Woudenbergh, C., Walker, G.S., Heerikhuisen, M., Nooijen, I.H.G., and Vaes, W.H.J. (2018). An ex vivo fermentation screening platform to study drug metabolism by human gut microbiota. Drug Metab. Dispos. 46, 1596–1607. https://doi. org/10.1124/DMD.118.081026.
- Ng, K.M., Aranda-Díaz, A., Tropini, C., Frankel, M.R., Van Treuren, W., O'Loughlin, C.T., Merrill, B.D., Yu, F.B., Pruss, K.M., Oliveira, R.A., et al. (2019). Recovery of the gut microbiota after antibiotics depends on host diet, community context, and environmental reservoirs. Cell Host Microbe 26, 650–665.e4. https://doi.org/10.1016/J.CHOM.2019. 10.011
- Newton, D.P., Ho, P.-Y., and Huang, K.C. (2022). Antibiotic effects on microbial communities are modulated by resource competition. Preprint at bioRxiv. https://doi.org/10.1101/2022.09.01.506215.
- Nagata, N., Nishijima, S., Miyoshi-Akiyama, T., Kojima, Y., Kimura, M., Aoki, R., Ohsugi, M., Ueki, K., Miki, K., Iwata, E., et al. (2022). Population-level metagenomics uncovers distinct effects of multiple medications on the human gut microbiome. Gastroenterology 163, 1038–1052. https://doi.org/10.1053/j.gastro.2022.06.070.
- Javdan, B., Lopez, J.G., Chankhamjon, P., Lee, Y.J., Hull, R., Wu, Q., Wang, X., Chatterjee, S., and Donia, M.S. (2020). Personalized mapping of drug metabolism by the human gut microbiome. Cell 181, 1661– 1679.e22. https://doi.org/10.1016/J.CELL.2020.05.001.
- Zimmermann, M., Zimmermann-Kogadeeva, M., Wegmann, R., and Goodman, A.L. (2019). Mapping human microbiome drug metabolism by gut bacteria and their genes. Nature 570, 462–467. https://doi.org/10. 1038/S41586-019-1291-3.
- Zimmermann, M., Zimmermann-Kogadeeva, M., Wegmann, R., and Goodman, A.L. (2019). Separating host and microbiome contributions to drug pharmacokinetics and toxicity. Science 363, eaat9931. https://doi. org/10.1126/SCIENCE.AAT9931.
- Lloyd-Price, J., Mahurkar, A., Rahnavard, G., Crabtree, J., Orvis, J., Hall, A.B., Brady, A., Creasy, H.H., McCracken, C., Giglio, M.G., et al. (2017).
 Strains, functions and dynamics in the expanded Human Microbiome Project. Nature 550, 61–66. https://doi.org/10.1038/nature23889.
- Le Chatelier, E., Nielsen, T., Qin, J., Prifti, E., Hildebrand, F., Falony, G., Almeida, M., Arumugam, M., Batto, J.-M., Kennedy, S., et al. (2013). Richness of human gut microbiome correlates with metabolic markers. Nature 500, 541–546. https://doi.org/10.1038/nature12506.
- Grießhammer, A., de la Cuesta-Zuluaga, J., Zahir, T., Müller, P., Gekeler, C., Chang, H., Schmitt, K., Planker, C., Bohn, E., Nguyen, T.H., et al. (2023). Non-antibiotic drugs break colonization resistance against pathogenic Gammaproteobacteria. Preprint at bioRxiv. https://doi.org/10.1101/ 2023.11.06.564936.
- Yoon, V., and Nodwell, J.R. (2014). Activating secondary metabolism with stress and chemicals. J. Ind. Microbiol. Biotechnol. 41, 415–424. https:// doi.org/10.1007/s10295-013-1387-y.
- Andersson, D.I., and Hughes, D. (2014). Microbiological effects of sublethal levels of antibiotics. Nat. Rev. Microbiol. 12, 465–478. https://doi. org/10.1038/nrmicro3270.
- Seyedsayamdost, M.R. (2014). High-throughput platform for the discovery of elicitors of silent bacterial gene clusters. Proc. Natl. Acad. Sci. USA 111, 7266–7271. https://doi.org/10.1073/pnas.1400019111.
- Spain, J.C. (1995). Biodegradation of nitroaromatic compounds. Annu. Rev. Microbiol. 49, 523–555. https://doi.org/10.1146/annurev.mi.49. 100195.002515.
- Roldán, M.D., Pérez-Reinado, E., Castillo, F., and Moreno-Vivián, C. (2008). Reduction of polynitroaromatic compounds: the bacterial nitroreductases. FEMS Microbiol. Rev. 32, 474–500. https://doi.org/10.1111/j. 1574-6976.2008.00107.x.
- Valiauga, B., Misevičiene, L., Rich, M.H., Ackerley, D.F., Šarlauskas, J., and Čenas, N. (2018). Mechanism of two-/four-electron reduction of nitroaromatics by oxygen-insensitive nitroreductases: the role of a





- non-enzymatic reduction step. Molecules 23, 1–9. https://doi.org/10.3390/MOLECULES23071672.
- Koder, R.L., Haynes, C.A., Rodgers, M.E., Rodgers, D.W., and Miller, A.F. (2002). Flavin thermodynamics explain the oxygen insensitivity of enteric nitroreductases. Biochemistry 41, 14197–14205. https://doi.org/10. 1021/Bi025805T.
- Akiva, E., Copp, J.N., Tokuriki, N., and Babbitt, P.C. (2017). Evolutionary and molecular foundations of multiple contemporary functions of the nitroreductase superfamily. Proc. Natl. Acad. Sci. USA 114, E9549–E9558. https://doi.org/10.1073/PNAS.1706849114.
- Wendel, A., Fausel, M., Safayhi, H., Tiegs, G., and Otter, R. (1984). A novel biologically active seleno-organic compound–II. Activity of PZ 51 in relation to glutathione peroxidase. Biochem. Pharmacol. 33, 3241–3245. https://doi.org/10.1016/0006-2952(84)90084-4.
- Luxo, C., Jurado, A.S., Madeira, V.M.C., and Silva, M.T. (2003). Tamoxifen induces ultrastructural alterations in membranes of Bacillus stearothermophilus. Toxicol. In Vitro 17, 623–628. https://doi.org/10.1016/S0887-2333(03)00113-9.
- Brown, R.E., Stancato, F.A., and Wolfe, A.D. (1979). The effects of mefloquine on Escherichia coli. Life Sci. 25, 1857–1864. https://doi.org/10.1016/0024-3205(79)90434-X.
- Wang, L., Zhou, W., Guo, M., Hua, Y., Zhou, B., Li, X., Zhang, X., Dong, J., Yang, X., Wang, Y., et al. (2021). The gut microbiota is associated with clinical response to statin treatment in patients with coronary artery disease. Atherosclerosis 325, 16–23. https://doi.org/10.1016/J.ATHEROSCLE-ROSIS.2021.03.007.
- Hu, X., Li, H., Zhao, X., Zhou, R., Liu, H., Sun, Y., Fan, Y., Shi, Y., Qiao, S., Liu, S., et al. (2021). Multi-omics study reveals that statin therapy is associated with restoration of gut microbiota homeostasis and improvement in outcomes in patients with acute coronary syndrome. Theranostics 11, 5778–5793. https://doi.org/10.7150/THNO.55946.
- Kummen, M., Solberg, O.G., Storm-Larsen, C., Holm, K., Ragnarsson, A., Trøseid, M., Vestad, B., Skårdal, R., Yndestad, A., Ueland, T., et al. (2020). Rosuvastatin alters the genetic composition of the human gut microbiome. Sci. Rep. 10, 5397. https://doi.org/10.1038/s41598-020-62261-y.
- Vancheri, F., Backlund, L., Strender, L.E., Godman, B., and Wettermark, B. (2016). Time trends in statin utilisation and coronary mortality in Western European countries. BMJ Open 6, e010500. https://doi.org/10.1136/ BMJOPEN-2015-010500.
- Gracia-Lor, E., Sancho, J.V., Serrano, R., and Hernández, F. (2012).
 Occurrence and removal of pharmaceuticals in wastewater treatment plants at the Spanish Mediterranean area of Valencia. Chemosphere 87, 453–462. https://doi.org/10.1016/j.chemosphere.2011.12.025.
- Barros, S., Montes, R., Quintana, J.B., Rodil, R., André, A., Capitão, A., Soares, J., Santos, M.M., and Neuparth, T. (2018). Chronic environmentally relevant levels of simvastatin disrupt embryonic development, biochemical and molecular responses in zebrafish (Danio rerio). Aquat. Toxicol. 201, 47–57. https://doi.org/10.1016/J.AQUATOX.2018.05.014.
- Barros, S., Coimbra, A.M., Alves, N., Pinheiro, M., Quintana, J.B., Santos, M.M., and Neuparth, T. (2020). Chronic exposure to environmentally relevant levels of simvastatin disrupts zebrafish brain gene signaling involved in energy metabolism. J. Toxicol. Environ. Health A 83, 113–125. https://doi.org/10.1080/15287394.2020.1733722.
- Tramontano, M., Andrejev, S., Pruteanu, M., Klünemann, M., Kuhn, M., Galardini, M., Jouhten, P., Zelezniak, A., Zeller, G., Bork, P., et al. (2018). Nutritional preferences of human gut bacteria reveal their metabolic idiosyncrasies. Nat. Microbiol. 3, 514–522. https://doi.org/10.1038/s41564-018-0123-9.
- Picard, C., Ponsonnet, C., Paget, E., Nesme, X., and Simonet, P. (1992).
 Detection and enumeration of bacteria in soil by direct DNA extraction and polymerase chain reaction. Appl. Environ. Microbiol. 58, 2717–2722. https://doi.org/10.1128/AEM.58.9.2717-2722.1992.

- Caporaso, J.G., Lauber, C.L., Walters, W.A., Berg-Lyons, D., Lozupone, C.A., Turnbaugh, P.J., Fierer, N., and Knight, R. (2011). Global patterns of 16S rRNA diversity at a depth of millions of sequences per sample. Proc. Natl. Acad. Sci. USA 108, 4516–4522. https://doi.org/10.1073/ PNAS.1000080107.
- Quast, C., Pruesse, E., Yilmaz, P., Gerken, J., Schweer, T., Yarza, P., Peplies, J., and Glöckner, F.O. (2013). The SILVA ribosomal RNA gene database project: improved data processing and web-based tools. Nucleic Acids Res. 41, D590–D596. https://doi.org/10.1093/NAR/GKS1219.
- Matias Rodrigues, J.F., Schmidt, T.S.B., Tackmann, J., and Von Mering, C. (2017). MAPseq: highly efficient k-mer search with confidence estimates, for rRNA sequence analysis. Bioinformatics 33, 3808–3810. https://doi.org/10.1093/BIOINFORMATICS/BTX517.
- Gloor, G.B., Macklaim, J.M., Pawlowsky-Glahn, V., and Egozcue, J.J. (2017). Microbiome datasets are compositional: and this is not optional. Front. Microbiol. 8, 2224. https://doi.org/10.3389/fmicb.2017.02224.
- Props, R., Kerckhof, F.-M., Rubbens, P., De Vrieze, J., Hernandez Sanabria, E., Waegeman, W., Monsieurs, P., Hammes, F., and Boon, N. (2017). Absolute quantification of microbial taxon abundances. ISME J. 11, 584–587. https://doi.org/10.1038/ismej.2016.117.
- 42. Mira, P., Yeh, P., and Hall, B.G. (2022). Estimating microbial population data from optical density. PLoS One 17, e0276040. https://doi.org/10.1371/journal.pone.0276040.
- Bullard, J.H., Purdom, E., Hansen, K.D., and Dudoit, S. (2010). Evaluation of statistical methods for normalization and differential expression in mRNA-Seq experiments. BMC Bioinformatics 11, 94. https://doi.org/10. 1186/1471-2105-11-94.
- Hughes, C.S., Moggridge, S., Müller, T., Sorensen, P.H., Morin, G.B., and Krijgsveld, J. (2019). Single-pot, solid-phase-enhanced sample preparation for proteomics experiments. Nat. Protoc. 14, 68–85. https://doi.org/ 10.1038/S41596-018-0082-X.
- Mateus, A., Hevler, J., Bobonis, J., Kurzawa, N., Shah, M., Mitosch, K., Goemans, C.V., Helm, D., Stein, F., Typas, A., et al. (2020). The functional proteome landscape of Escherichia coli. Nature 588, 473–478. https://doi. org/10.1038/s41586-020-3002-5.
- Huber, W., Von Heydebreck, A., Sültmann, H., Poustka, A., and Vingron, M. (2002). Variance stabilization applied to microarray data calibration and to the quantification of differential expression. Bioinformatics 18, S96–S104. https://doi.org/10.1093/BIOINFORMATICS/18. SUPPL 1.S96.
- Bateman, A., Martin, M.J., Orchard, S., Magrane, M., Agivetova, R., Ahmad, S., Alpi, E., Bowler-Barnett, E.H., Britto, R., and Bursteinas, B. (2021). UniProt: the universal protein knowledgebase in 2021. Nucleic Acids Res. 49, D480–D489. https://doi.org/10.1093/NAR/GKAA1100.
- Whitaker, W.R., Shepherd, E.S., and Sonnenburg, J.L. (2017). Tunable expression tools enable single-cell strain distinction in the gut microbiome. Cell 169, 538–546.e12. https://doi.org/10.1016/j.cell.2017.03.041.
- Bobonis, J., Yang, A.L.J., Voogdt, C.G.P., and Typas, A. (2024). TAC-TIC, a high-throughput genetics method to identify triggers or blockers of bacterial toxin-antitoxin systems. Nat. Protoc. 19, 2231–2249.
- Ruscheweyh, H.-J., Milanese, A., Paoli, L., Karcher, N., Clayssen, Q., Keller, M.I., Wirbel, J., Bork, P., Mende, D.R., Zeller, G., et al. (2022). Cultivation-independent genomes greatly expand taxonomic-profiling capabilities of mOTUs across various environments. Microbiome 10, 212. https://doi.org/10.1186/s40168-022-01410-z.
- Parks, D.H., Chuvochina, M., Rinke, C., Mussig, A.J., Chaumeil, P.-A., and Hugenholtz, P. (2022). GTDB: an ongoing census of bacterial and archaeal diversity through a phylogenetically consistent, rank normalized and complete genome-based taxonomy. Nucleic Acids Res. 50, D785–D794. https://doi.org/10.1093/nar/gkab776.





STAR***METHODS**

KEY RESOURCES TABLE

REAGENT or RESOURCE	SOURCE	IDENTIFIER
Bacterial and virus strains		
Akkermansia muciniphila	DSMZ	DSM 22959
Bacteroides fragilis	DSMZ	DSM 2151
Bacteroides thetaiotaomicron	DSMZ	DSM 2079
Bacteroides uniformis	DSMZ	DSM 6597
Bifidobacterium adolescentis	DSMZ	DSM 20083
Bifidobacterium longum subsp. longum	DSMZ	DSM 20219
Bilophila wadsworthia	ATCC	ATCC 49260
Blautia obeum	DSMZ	DSM 25238
Clostridium perfringens	DSMZ	DSM 11782
Collinsella aerofaciens	DSMZ	DSM 3979
Coprococcus comes	ATCC	ATCC 27758
Dorea formicigenerans	DSMZ	DSM 3992
Eggerthella lenta	DSMZ	DSM 2243
Enterocloster bolteae	DSMZ	DSM 15670
Erysipelatoclostridium ramosum	DSMZ	DSM 1402
Escherichia coli ED1a	Denamur Lab, INSERM	N/A
Eubacterium rectale	DSMZ	DSM 17629
Fusobacterium nucleatum subsp. nucleatum	DSMZ	DSM 15643
Lacrimispora saccharolytica	DSMZ	DSM 2544
Lacticaseibacillus paracasei	Dupont Health and Nutrition	N/A
Odoribacter splanchnicus	DSMZ	DSM 20712
Parabacteroides distasonis	DSMZ	DSM 20701
Parabacteroides merdae	DSMZ	DSM 19495
Phocaeicola vulgatus	DSMZ	DSM 1447
Prevotella copri	DSMZ	DSM 18205
Roseburia intestinalis	DSMZ	DSM 14610
Ruminococcus bromii	ATCC	ATCC 27255
Ruminococcus gnavus	ATCC	ATCC 29149
Ruminococcus torques	ATCC	ATCC 27756
Streptococcus parasanguinis	DSMZ	DSM 6778
Streptococcus salivarius	DSMZ	DSM 20560
Veillonella parvula	DSMZ	DSM 2008
EC100D pir+ RP4-2-Tc::[ΔMu1::aac(3)IV- ΔaphA-Δnic35-ΔMu2::zeo] 903 ΔdapA::hygromycin	DSMZ	DSM 116187
Nitroreductase overexpression strains, Table S1	This study	N/A
Chemicals, peptides, and recombinant proteins		
Acarbose	TCI Deutschland GmbH	Cat#A2485
Amlodipine	TCI Deutschland GmbH	Cat#A2353
Aprepitant	TCI Deutschland GmbH	Cat#A3135
Aripiprazole	TCI Deutschland GmbH	Cat#A2496
Azithromycin	Sigma	Cat#75199

(Continued on next page)





Continued		
REAGENT or RESOURCE	SOURCE	IDENTIFIER
beta-estradiol 17-valerate	TCI Deutschland GmbH	Cat#E0876
Chlorpromazine	TCI Deutschland GmbH	Cat#C2481
Ciprofloxacin	Sigma	Cat#17850
Clomiphene	Sigma	Cat#C6272-1G
Diacerein	Santa Cruz Biotechnology	Cat#sc-204717
Dienestrol	TCI Deutschland GmbH	Cat#D0449
Doxyxycline	Sigma	Cat#D9891
Ebselen	TCI Deutschland GmbH	Cat#E0946
Entacapone	Sigma	Cat#SML0654
Felodipine	TCI Deutschland GmbH	Cat#F0814
Ketoconazole	TCI Deutschland GmbH	Cat#K0045
_ansoprazole	TCI Deutschland GmbH	Cat#L0233
_oratadine	TCI Deutschland GmbH	Cat#L0223
_oxapine	Sigma	Cat#L106
Mecillinam	Sigma	Cat#33447
Mefloquine	TCI Deutschland GmbH	Cat#M2313
Methotrexate	TCI Deutschland GmbH	Cat#M1664
Viclosamide	Sigma	Cat#N3510-50G
Vifurtimox	Sigma	Cat#N3415-5MG
Olanzapine	TCI Deutschland GmbH	Cat#00393
Omeprazole	TCI Deutschland GmbH	Cat#00359
Oxolinic acid	Santa Cruz Biotechnology	Cat#sc-212488
Sertindole	TCI Deutschland GmbH	Cat#S0942
Simvastatin	Santa Cruz Biotechnology	Cat#sc-200829A
Famoxifen	Santa Cruz Biotechnology	Cat#sc-203288
N-(4-amino-2-chlorophenyl)-5-chloro-2- nydroxybenzamide	Sigma	Cat#EN300-209216
Niclosamide-(2-chloro-4-nitrophenyl- 13C6) hydrate	Sigma	Cat#35365
2-amino-N-(4-chlofophenyl)benzamide	Sigma	Cat#TMT00102-1G
Warfarin , , , , , , , , , , , , , , , , , , ,	Sigma	Cat#A2250-10G
Caffeine	Sigma	Cat#C0750
priflavone	Sigma	Cat#16499
Sulfamethoxazole	TOKU-E	Cat#S045
GAM Broth, modified	HyServe GmbH & Co.KG	Cat#05433
Fodd Hewitt broth	Sigma	Cat#T1438
SYBR™ Master Mix	Applied Biosystems	Cat#43-091-55
Critical commercial assays	· ·	
DNA extraction kit GNOME00E2 DNA	MP Biomedicals	Cat#2010400
Deposited data		
Raw 16S amplicon sequencing data	N/A	ENA: PRJEB63118.
LC-MS community metabolomics data	N/A	Metabolights https://www.ebi.ac.uk/
LO-IVIO COMMUNICY METADOIOMICS CATA		metabolights/: MTBLS10112
Oligonucleotides		
Primers for qPCR, see Table S3	This paper	N/A
Primers for nitroreductases	This paper	N/A
overexpression, see Table S3		

(Continued on next page)





Continued		
REAGENT or RESOURCE	SOURCE	IDENTIFIER
Recombinant DNA		
Plasmids for nitroreductases overexpression, see Table S3	This paper	N/A
Software and algorithms		
MassHunter Quantitative Analysis Software 10.0	Agilent Technologies	N/A
isobarQuant	Matrix Science	N/A
Mascot 2.4	Matrix Science	N/A
Other		
Data availability	This paper	https://github.com/grp-bork/drugbug_ Santamarina_2023
Code availability	This paper	https://github.com/grp-bork/drugbug_ Santamarina_2023

EXPERIMENTAL MODEL

Bacterial species and growth conditions

Species used in this study were purchased from DSMZ, BEI Resources, ATCC and Dupont Health & Nutrition, or were gifts from the Denamur Laboratory (INSERM) and processed as previously described.³ All species (monoculture or community) were grown in mGAM (HyServe GmbH & Co.KG, Germany) except the monocultures of *Veillonella parvula* and of *Bilophila wadsworthia*, which were grown in Todd-Hewitt Broth supplemented with 0.6% sodium lactate and mGAM supplemented with 60 mM sodium formate and 10 mM taurine, respectively. Media was pre-reduced to a minimum of 24 h under anoxic conditions (2% H₂, 12% CO₂, 86% N₂) in an anaerobic chamber (Coy Laboratory Products Inc.). Experiments were performed at 37°C and under anaerobiosis, species were inoculated from frozen stocks into liquid culturing media, and passaged twice overnight to ensure robust growth, and drug stocks in DMSO were prereduced overnight in the anaerobic chamber inside an ice-box at 4°C. A representative core of species in the human gut microbiome were selected as previously described.^{3,35} From this core, 32 diverse species, differing more than 1.35% on their 16S rDNA sequences at the V4 region, were selected for the screening.

METHOD DETAILS

Chemical screening of a bottom-up assembled bacterial community of 32 species Screening plate preparation

Drugs were dissolved with the appropriate solvent (i.e., 100% DMSO), except for oxolinic acid and ciprofloxacin, which were dissolved with 0.5 M NaOH and 0.1M HCl, respectively (Table S1, at a concentration 100-fold higher than the screening concentration, distributed in 96-well V-bottom plates (Greiner, 651261), each well containing 11 µl of dissolved compound or vehicle (100% DMSO), and stored at -30°C for up to 1 month. One day before the experiment, drug plates were thawed, and each of the 11 µl of drug or vehicle per well were added to 539 µl/well of mGAM in 96-deep well plates (Costar 3959) using the Biomek FXP (Beckman Coulter) liquid handling system. These plates were pre-reduced in the anaerobic chamber overnight ("Community Plates Day1"). Inoculation of community passage 1. For community assembly, the optical density (OD) was individually measured at 578 nm for the 32 species. These were added together into 200 ml of mGAM with the volume required to reach a total of 2x the desired initial OD of 0.01: therefore, each species was added at an OD of 0.0006. 550 μl of the assembled community was added into each well of the "Community Plates Day 1" with an epMotion 96 (Bio-Rad) semi-automated electronic 96 channel pipette. Final drug concentrations are described in Table S1 and each well contained 1% DMSO. After inoculation, 100 µl/well were transferred from the "Community Plates Day 1" to U-bottom shallow 96-well plates ("Community Growth Plates Day 1") (Fisher Scientific 168136), sealed with breathable membranes (Breathe-Easy, Sigma), and incubated at 37°C. These plates were used for monitoring community growth after drug treatment, for which OD₅₇₈ was measured with a microplate spectrophotometer (EON, Biotek) every hour during 24 h, with shaking only few seconds before OD measurement. The "Community Plates Day 1" were also sealed with a breathable membrane (AeraSeal, Sigma) and incubated during 24 h. The untreated community grew to an average OD₅₇₈ of 1 (7 generations). Inoculation of community passage 2. After the initial 24 h incubation, the drug-treated community was passaged with a 1:50 dilution (OD₅₇₈ of 0.02 for the untreated community) into a new drug-containing deep-well plate for an additional 24 h incubation as follows: during the initial 24 h incubation period, new drug plates were thawed, and the 11 μl of drug or vehicle was added to 1067 μl/well of mGAM in 96-deep well plates ("Community Plates Day 2"). These were prereduced in the anaerobic chamber overnight. Wells in the "Community Plates Day 1"





were mixed with the 96 channel epMotion pipette, and from here 22 μl were transferred to the "Community Plates Day 2". Of these, 100 μl were transferred to 96-well U-bottom plates ("Community Growth Plates Day 2"), for growth curve acquisition, as described above. The "Community Plates Day 2" were incubated for 24 h anaerobically and at 37°C. The untreated community grew to an average OD₅₇₈ of 1 (5-6 generations). After 24 h of incubation, cell pellets were collected by centrifugation. DNA extraction and 16S rDNA sequencing were performed as described below. These experiments were performed in 3 biological replicates (different days: different community assemblies, batch of media) with 2 technical replicates each (same community assembly and batch of media, but distinct culture/well of plate).

Genomic DNA isolation

Genomic DNA isolation was done as previously described. Briefly, DNA was extracted in a 96-well plate format using a Biomek FXP (Beckman Coulter) liquid handling system or in single tubes depending on the number of samples. Cells were first washed with PBS and resuspended in 281 μ l of cell suspension solution (MP GNOME DNA kit). Cell suspension was treated with lysozyme (25 μ l; 400.000 U/ml) and incubated for 1 h at 37 °C. Cell suspensions were then further lysed by three freeze/thaw cycles using liquid nitrogen, before the addition of 15.2 μ l of cell lysis solution (MP GNOME DNA kit) and 20 μ l of RNA mix (MP GNOME DNA kit). A last step of lysis was performed using glass beads (Glasperlen, Edmund Bühler) by bead beating twice for 5 min at 30 Hz in a Tissue Lyzer II (QIAGEN). Lysates were then incubated for 30 min at 37 °C with shaking. 12.8 μ l of protease mix (MP GNOME DNA kit) was subsequently added and the lysates were incubated for 2 h at 55 °C. After a 5-min centrifugation step at 3.200 x g, 200 μ l of supernatants were collected and mixed with 100 μ l of TENP buffer (buffer: 50 mM Tris-HCl, pH=8, 20 mM EDTA, 100 mM NaCl, 1% w/vol polyvinlylpolypyrrolidone), and with 75 μ l salt out solution (MP GNOME DNA kit). These were incubated for 10 min with at 4 °C. After a 10 min centrifugation at 3200 x g, 200 μ l of supernatant were transferred to a clean plate. 500 μ l of ice-cold ethanol and 70 μ l of 3M NaOAc pH 5.2 were added. The solution was kept at -30 °C overnight. The next day, the plates were centrifuged at 4 °C, 3.200 x g for 45 min. The supernatant was carefully removed and the pellets were washed with 400 μ l of ice-cold 70% ethanol. After a 20 min centrifugation at 3200 x g at 4 °C, all the supernatant was removed and plates were dried in a chemical hood for 30 min. DNA was resuspended in 70 μ l water overnight at 4 °C.

16S rDNA sequencing

The 16S libraries were then prepared for sequencing using a published two-step PCR method, ³⁷ using the Phire Hot Start II DNA polymerase (Thermo Scientific). Briefly, the V4 region was amplified by a first PCR with the 515F/806R primers (Table S3). The resulting amplicons were subsequently amplified again using barcoded primers that contain Illumina adaptors. These libraries were sequenced in the EMBL GeneCore sequencing facility on an Illumina MiSeq (250 base pairs, paired-end).

Processing of 16S data and quantification of species abundances

To estimate the species abundance, a database of 16S rRNA regions was constructed by manually querying the SILVA rRNA database³⁸ and extracting the representative sequence from each of our 32 species. Amplicon sequencing reads were then mapped against this database using MAPseq v1.2.³⁹ Paired reads were mapped independently and assignments were only considered upon agreement. Abundance estimates were then produced by counting the number of reads mapping to each genome included in the study. Eleven species whose median read count in controls was below 10 were designated as rare species and excluded from the subsequent analysis, as for these species abundance ratios would be unreliable. Relative species abundances were calculated by dividing the number of reads mapping to each species by the total number of reads for a sample.

As 16S sequencing data are compositional,⁴⁰ we estimated absolute species abundances using the final OD of the community.^{41,42} We set the controls' OD to 1 and multiplied each condition's OD by the relative species abundances. In this way, the normalized species abundances sum to 1 for controls, and to lower values when drug treatment has inhibited the overall growth of the community. To ensure that relying on OD as a proxy for cell counts does not lead to large distortions, we also calculated standardized relative abundances by dividing the relative abundances within each condition by the 75th percentile of the relative abundances, also known as upper-quartile normalization.⁴³ We chose the 75th percentile instead of the median, as this is more robust to the case where the growth of many species is inhibited.

Quantification of treatment effects

Control abundances were separately determined for each biological and technical replicate by calculating the mean abundance across six control wells. For each species and treatment condition, we calculated the ratio of treatment and control abundances to estimate the effect of drug treatment on each species independently of its absolute abundance. Species whose abundance was decreased to 50% or less upon drug treatment were designated as being reduced in the community.

Community metabolomics

LC-MS analyses were employed to assess the presence/absence of a drug after incubation with the community of 30 species (compared to the initial community, *Ruminococcus bromii*, and *Ruminococcus torques*, which did not grow reliably in the community, were not added as cells did not grow from stocks). Drug plates, community assembly, passages, and incubations were performed as described above, with the only exception that the community inoculation in the 2nd passage was performed in a final volume of 1.5 ml per well. Final drug concentrations are listed in Table S1. Immediately after inoculating the community in the 2nd passage: i) 100 μl were transferred to 96-well U-bottom plates for growth curve acquisition, as described above, ii) 100 μl were transferred to 96-well shallow U-bottom plates and immediately stored frozen at -80 °C (0 h time point), and iii) 150 μl were transferred to 5 different 96-well shallow U-bottom plates, which were incubated anaerobically at 37 °C for





1.15 h, 2.5 h, 5 h, 7.5 h, and 10 h, respectively. At each time point, 75 μl/well were transferred to a new plate and immediately frozen at -80 °C (cells and supernatants), the remaining 75 µl/well were centrifuged for 5 min at 4.680 rpm in an Eppendorf 5430 centrifuge, and 50 μl of the supernatants transferred to a new plate, which was immediately frozen at -80 °C (supernatants). To assess drug stability in the culture media (mGAM), drugs were pooled together in three different pools according to drug-treatment concentration: 80 uM, 20 and 30 uM, and 2.5 and 5 uM. Immediately after pooling the drugs, 1) 100 μl were transferred to 96-well shallow U-bottom plates and immediately stored frozen at -80 °C (0 h time point), and 2) 150 μl were transferred to 5 different 96-well U-bottom plates, which were incubated anaerobically at 37 °C for 1.15 h, 2.5 h, 5 h, 7.5 h, and 10 h, respectively. At each time point, the plates were immediately frozen at -80 °C. Metabolite extraction. Frozen samples were thawed on ice, and 20 μl of supernatants, cells and supernatants or of mGAM were distributed into 96-well plates (V-bottom storage plates, Thermo Scientific) according to drug-treatment concentration: 80 uM, 20 and 30 uM, and 2.5 and 5 uM. Additionally, 20 µl of pooled drug stocks, split according to the concentration range, were serial diluted in fresh mGAM to set-up calibration curves in all plates. Pooled ¹³C-niclosamide, warfarin, caffeine, ipriflavone, 2-amino-N-cholrophenyl)benzamide (Sigma), and sulfamethoxazole (TOKU-E) were diluted in 50% DMSO and used as internal standards (IS) by adding 5 µl per well of 160 uM, 40 uM, and 10 uM stock concentrations to the 80 uM, 20 and 30 uM, and 2.5 and 5 uM sample plates, respectively. For metabolite extraction, 100 µl/well of a 1:1 mix of methanol:acetonitrile were added using the Biomek FXP (Beckman Coulter) liquid handling system. Well contents were mixed and plates were incubated at -20 °C overnight. After incubation, samples were centrifuged at 4.000 rpm in a 5810R Eppendorf centrifuge for 10 min at 4 °C. 80 uM, 20 and 30 uM, and 2.5 and 5 uM treated samples were diluted 1/7, 1/2, and 2/1, respectively, with H₂O for analysis by LC-MS. These experiments were performed in 2 biological replicates with 2 technical replicates each. LC-MS measurements. Chromatographic separation was performed using an Agilent InfinityLab Poroshell HPH-C18 1.9 µM, 2.1 x 10 mm column and an Agilent 1290 Infinity II LC system coupled to a 6546 Q-TOF mass spectrometer. Column temperature was maintained at 45 °C with a flowrate of 0.6 ml/min. The following mobile phases were used: mobile phase A: water with 0.1% formic acid and mobile Phase B: acetonitrile with 0.1% formic acid. 5 mL of sample were injected at 5% mobile phase B, maintained for 0.10 min, followed by a linear gradient to 95% B in 5.5 min and maintained at 95% B for 1 min. The column was allowed to re-equilibrate with starting conditions for 0.5 min before each sample injection. The mass spectrometer was operated in positive mode (50-1,700 m/z) with the following source parameters: VCap, 3,500 V; nozzle voltage, 2000 V; gas temperature, 275 °C; drying gas 13 l/min; nebulizer, 40 psi; sheath gas temperature 275 °C; sheath gas flow 12 I/min, fragmentor, 365 V and skimmer, 750 V. Online mass calibration was performed using a second ionization source and a constant flow (10 μL/min) of reference mass solvent (121.0509 and 922.0098 for positive). Quantification of compounds was performed using the MassHunter Quantitative Analysis Softwere (Aglient Technologies, version 10.0). For niclosamide, we used the same method as we reported for single species metabolomics (see below). During data processing, one of the internal standards was selected to normalize the compound's signal based on the correlation between the measured signal and the expected concentration.

Chemical screening of bacterial monocultures Screening plate preparation

Drugs were dissolved with the appropriate solvent (Table S1) at a concentration 200-fold higher than the screening concentration, distributed in 96-well V-bottom plates (Greiner, 651261), each well containing 10 μ I of dissolved compound or vehicle, and stored at -30°C for up to 1 month. Before the experiment, drug plates were pre-reduced overnight in the anaerobic chamber inside an ice-box at 4 °C. The experiment day, the 10 μ I of drug or vehicle was added to 990 μ I/well of media in 96-deep well plates (Costar 3959) and 50 μ I/well were transferred to shallow U-bottom 96-well plates using the epMotion 96 (Bio-Rad) semi-automated electronic 96 channel pipette.

Species inoculation

Species, started in liquid media from a -80 °C glycerol stock, were passaged twice overnight. For inoculation, the second overnight culture was diluted into fresh medium to an OD_{578} of 0.02 (2x). 50 μ l/well were added to the 96-well U-bottom drug containing plates, to final drug concentrations as indicated in Table S1, 1% DMSO, and starting bacterial cultures at OD_{578} of 0.01. Plates were sealed with breathable membranes and incubated at 37 °C, with shaking only a few seconds before OD measurement, as described above. These experiments were performed in 3 biological replicates with 2 technical replicates each.

Single-species growth curves

Growth curves for single species were determined for the 21 species that were consistently detected in the *in vitro* communities (Table S1). As previously described, ³ growth curves were quality-controlled, and truncated at the end of the exponential phase under control conditions. The AUC was calculated for all conditions and divided by the median control AUC within each plate. Across all treatment conditions, the standard deviation between biological and technical replicates had a mean value of 0.04 and 0.03, respectively. In our previous screen, ³ a large number of control wells and wells with inactive drugs made it possible to calculate a distribution of AUCs for normal growth, and to calculate *p* values based on this distribution. In this more focused screen with no inactive drugs and fewer control wells, this was not possible and we therefore opted to use an AUC threshold of 0.75 (i.e., a substantial growth reduction by 25%) to determine whether a species was susceptible to drug treatment.





Single-species metabolomics

LC-MS measurements were employed to assess the presence/absence of a drug or a drug metabolite after incubation with a single-species culture. A 96-deep well plate was filled with 750 µl/well of a 2x drug concentration in mGAM. Inoculation was performed by filling the plate with 750 µl/well of mGAM containing different species at OD₅₇₈ of 0.02, as indicated. Immediately after species inoculation: (1) 100 μl were transferred to 96-well U-bottom plates for growth curve acquisition, as described above, (2) 100 μl were transferred to 96-well U-bottom plates and immediately stored frozen at -80 °C (0 h time point), and (3) 100 μl were transferred to different 96-well U-bottom plates, which were incubated anaerobically at 37 °C for the indicated times. At each time point, plates were immediately frozen and stored at -80 °C until metabolite extraction. Metabolite extraction. Frozen samples were thawed on ice, and 20 μl of the samples were distributed into 96-well plates (V-bottom storage plates, Thermo Scientific). Additionally, 20 µl of pooled niclosamide and aminoniclosamide, or of nifurtimox were serial diluted in fresh mGAM to set-up calibration curves. Pooled 2-amino-N-cholrophenyl)benzamide and 13C-niclosamide (Sigma) were diluted in 50% DMSO and used as internal standards (IS) by adding 5 µl per well of 2x drug treatment respectively. Metabolite extraction was performed with methanol:acetonitrile as described above. These experiments were performed at least in 2 biological replicates with 2 technical replicates each. When specified, drug bioaccumulation was analyzed by splitting supernatants from cells and supernatants by centrifugation right after time point collection and before freezing at -80 °C, as described above for the community metabolomics. Bioaccumulated drug concentration was calculated by subtracting the drug concentration obtained from the cell and supernatant fraction minus the drug concentration in the supernatant fraction. LC-MS measurements. Chromatographic separation was performed using an Agilent InfinityLab Zorbax Eclipse Plus C18, 1.8mM, 2.1 x 50mm column and an Agilent 1290 Infinity II LC system coupled to a 6546 Q-TOF mass spectrometer. Column temperature was maintained at 45 °C with a flow rate of 0.6 ml/min. The following mobile phases were used: Mobile phase A: Water with 0.1% Formic acid and mobile Phase B: Acetonitrile with 0.1% Formic acid. 5 mL of sample were injected at 5% mobile phase B, maintained for 0.10 min, followed by a linear gradient to 20% B in 0.4 min, followed by a linear gradient to 95% B in 4 min and maintained at 95% B for 0.5 min. The column was allowed to re-equilibrate with starting conditions for 0.5 min before each sample injection. The mass spectrometer was operated in positive mode for initial 3.6 min and then switched to negative scanning mode (50-1,700 m/z) with the following source parameters: VCap, 4,000 V; nozzle voltage, 1000 V; gas temperature, 290 °C; drying gas 13 l/min; nebulizer, 50 psi; sheath gas temperature 400 °C; sheath gas flow 12 l/min, fragmentor, 130 V and skimmer, 750 V. Online mass calibration was performed using a second ionization source and a constant flow (10 μL/min) of reference mass solvent (121.0509 and 922.0098 for positive and 119.0363 and 1033.9881 m/z for negative operation mode, respectively). Quantification of compound was performed using the MassHunter Quantitative Analysis Softwere (Aglient Technologies, version 10.0).

Quantification of community effects Protection and sensitization

The assessment of the effects of the community on the drug sensitivity of individual species is based on the comparison of the expected behavior in bacterial monocultures and the observed treatment effects in the bacterial community. To compute the fraction of species that are protected in the community for a certain treatment condition, we only considered the subset of species that are affected by the drug in the monoculture experiment. For this subset of species, we divided the number of species that grew normally in the community by the number of affected species. Conversely, to determine the fraction of species that are cross-sensitized in the community, we divided the number of species that showed reduced growth in the community (but grew normally in monoculture) by the number of species that grew normally in the monoculture experiment. For some species, the growth reduction was close to the designated threshold, and in some replicates the growth might be counted as reduced while in others as normal. We therefore counted each technical replicate individually in the calculation of the fractions of affected species, instead of combining them first.

Concentration dependency

The concentration dependency of the community effects was calculated both on the concentration steps of the drug (low/middle/high) and the actual numerical concentration. In the first instance, we determined for each drug the concentration steps for which the community effect could be determined. For example, consider a drug which only reduced the growth of any species monoculture at its middle and high concentration but not at its lowest concentrations. For determining the concentration dependency, these would be considered as the low and middle concentration. The distributions of the fractions of affected species were compared using Wilcoxon signed-rank tests.

In addition, we fitted separate logistic functions for sensitization and protection for all drugs which were affected at more than one concentration step. Parameters are a common growth rate k and drug-specific offset d_i to capture the relation between the fraction of affected species $f_{i,j}$ for the concentration step $c_{i,j}$:

$$f_{i,j} = \left(1 + e^{-k\left(\log c_{i,j} - d_i\right)}\right)^{-1}$$

We compared the resulting model with a simplified model that has no concentration dependency, i.e., only one constant value for each drug. We ascertained that the concentration-dependent model provides a better fit to the data using both an ANOVA (analysis of variance) and the BIC (Bayesian information criterion), Figure S3.





Spent media experiments

Spent media experiments were used to evaluate specie's effects on drugs and whether these protect (potential protectors) other species (drug-sensitive species) from drug toxicity. All species were inoculated from glycerol stocks into liquid medium, passaged for two days, and diluted to final OD_{578} of 0.01 to perform the experiments. Potential protectors and mGAM controls were grown, for the indicated times, in the presence of 2x the indicated drug concentrations. After the incubation periods, the potential protectors and mGAM controls were sterilized with 0.22 μ m PVDF filters (Millipore). 50% of the filtrate (growth spent media) was diluted with 50% of fresh mGAM containing drug-sensitive species at OD_{578} of 0.02 in shallow 96-well U-bottom drug-containing plates. The final drug concentrations are as indicated in the figures. Plates were sealed with breathable membranes and incubated at 37°C for monitoring the growth of the sensitive species every hour during 24 h, as described above. These experiments were performed at least in 3 biological replicates with 2 technical replicates each.

Small community growth rescue by a drug detoxifier

Two small bacterial communities assembled by mixing *Bacteroides uniformis*, *Bifidobacterium longum*, *Streptococcus parasanguinis*, *S. salivarius* with and without *Coprococcus comes* at a starting OD₅₇₈ nm of 0.01 were kept untreated or treated with 10 μM niclosamide for 24 h. At 24 h pellets were collected by centrifugation and DNA was isolated and bacterial community composition was quantified by qPCR. Community growth was monitored in 96-well U-bottom plates as described above.

Bacterial community composition quantification by qPCR

Primer design. Species-specific primers were designed using the NCBI primer design tool by selecting the following common parameters: product length of 200 bp maximum, 25 bp primer length, Tm 70 °C ± 3 °C, G/C content < 60%. Primers were tested in silico for homology to non-specific sites against nr and RefSeg representative genomes by BLAST, and in vitro by PCR against genomic DNA isolated from each individual species included in the community. The 515F/806R primers³⁷ (Table S3) targeting the V4 hypervariable regions of 16S rDNA were used for the amplification of the 16S rDNA of the community in each sample. Four-point standard curves were prepared from ten-fold serial dilutions of DNA prepared for each individual species, starting at concentration of ~1 ng/μL using 1 μL per well in duplicate reactions (range from ~1 ng – 2 pg). The standard curves demonstrated good linearity in four orders of magnitude (R^2 of 0.989-1.000) for all DNAs except for DNA isolated from B. uniformis, where linearity was three orders of magnitude. Species specific primer's efficiencies ranged from 91 to 100 %, 16S rDNA primer's efficiencies were 84.5% ± 5.5%. Reaction conditions. 20 μL qPCR reactions containing 10 μL SYBR™ master mix (Applied Biosystems), 1 μL nuclease-free water, 4 μL of 4 μM primer mix (0.2 μM each final), and 1 μL of template DNA (5-10 ng) were run on 96-well plates on a StepOne Plus Real-Time PCR system (ThermoFisher Scientific). A melting curve analysis was carried out to confirm the amplification of a single product in each reaction. Data analysis. Normalized DNA contributed by each species per condition was determined by calculating the threshold cycle (ΔΔCT) value for each gene in relation to the 16S rDNA of the community. To reflect the effect of the community growth on the final community composition, the resulting normalized DNA value was divided by the final OD₅₇₈ of the community at 24 h.

Overexpression of nitroreductases

Proteomics

For proteomics experiments, overnight cultures of the different species were diluted to an OD_{578} 0.1, and anaerobically grown until $OD_{578}\sim1$. At this point, cell cultures were treated with vehicle (DMSO) or $20~\mu\text{M}$ niclosamide for 30 minutes. Cell pellets were collected by 10 min centrifugation at 4000 x g, washed with ice-cold PBS, and frozen at -80°C until further processing. Cells were then resuspended in a lysis buffer (2% SDS, 250 U/ml benzonase, and 1 mM MgCl₂ in PBS) and boiled at 95 °C for 10 min. After measuring protein concentration using the BCA assay, according to the manufacturer's instructions (ThermoFisher Scientific), 5 μ g of protein from each condition were digested using a modified SP3 protocol⁴⁴ as previously described.⁴⁵ Peptides were labeled with TMT10plex (Thermo Fisher Scientific), fractionated under high pH conditions, and analyzed using liquid chromatography coupled to tandem mass spectrometry, as previously described.⁴⁵ Mass spectrometry data were processed using isobarQuant and Mascot 2.4 (Matrix Science) against the *R. intestinalis* (UP000004828) and *P. vulgatus* (UP000002861) UniProt FASTA. Protein abundance (niclosamide treated samples vs vehicle control) was calculated after normalizing the signal sum intensity across conditions using vsn.⁴⁶

Nitroreductases over-expressing species

Annotated *R. intestinalis* (UP000004828) and *P. vulgatus* (UP000002861) nucleotide sequences of nitroreductases were retrieved from the genome annotation databases from UniprotKB. The Plasmids were constructed by Gibson assembly reactions, using the plasmid pww3864 as a backbone, which were transformed into the chemically competent *E. coli* species EC100. For this, PCRs using the primer sequences described in Table S3 were used to amplify the vector pww3864 and the nitroreductases ORFs from extracted genomic DNA. Resulting plasmids and pww3864 were electroporated into the *E. coli* conjugation donor species EC100D pir+ RP4-2-Tc::[Δ Mu1::aac(3)IV- Δ aphA- Δ nic35- Δ Mu2::zeo] Δ dapA::hygromycin. For conjugating the nitroreductases plasmids from the *E. coli* donor into the recipient *P. vulgatus*, overnight aerobic cultures of donor species (grown in LB + 0.3 mM diaminopimelic acid (DAP) + 100 μ g/ml ampicillin) and anaerobic cultures of *P. vulgatus* (grown in mGAM) were diluted 50- and 20-fold respectively, and grown for 3 h. At 3 h, cells were collected by centrifugation and donor cells were washed 3 times with LB. Cells were resuspended in 200 μ l of mGAM, and 25 μ l of each donor species was mixed with 25 μ l of the recipient





P.~vulgatus, plated on mGAM plates supplemented with 0.3 mM DAP, and incubated at 37 °C overnight aerobically. After overnight incubation, cells were collected and plated on mGAM plates supplemented with erythromycin (10 μ g/ml) and gentamicin (200 μ g/ml). P.~vulgatus transconjugants were confirmed by PCR.

Calculation of species abundances in human microbiomes

Relative species abundances were calculated from the raw sequencing data using the mOTUs profiler (version 3).⁵⁰ Unassigned reads and samples with insert counts below 1000 were discarded. Species were mapped to the GTDB (release 207),⁵¹ and relative species abundances were collated on the species and genus level.



Supplemental figures

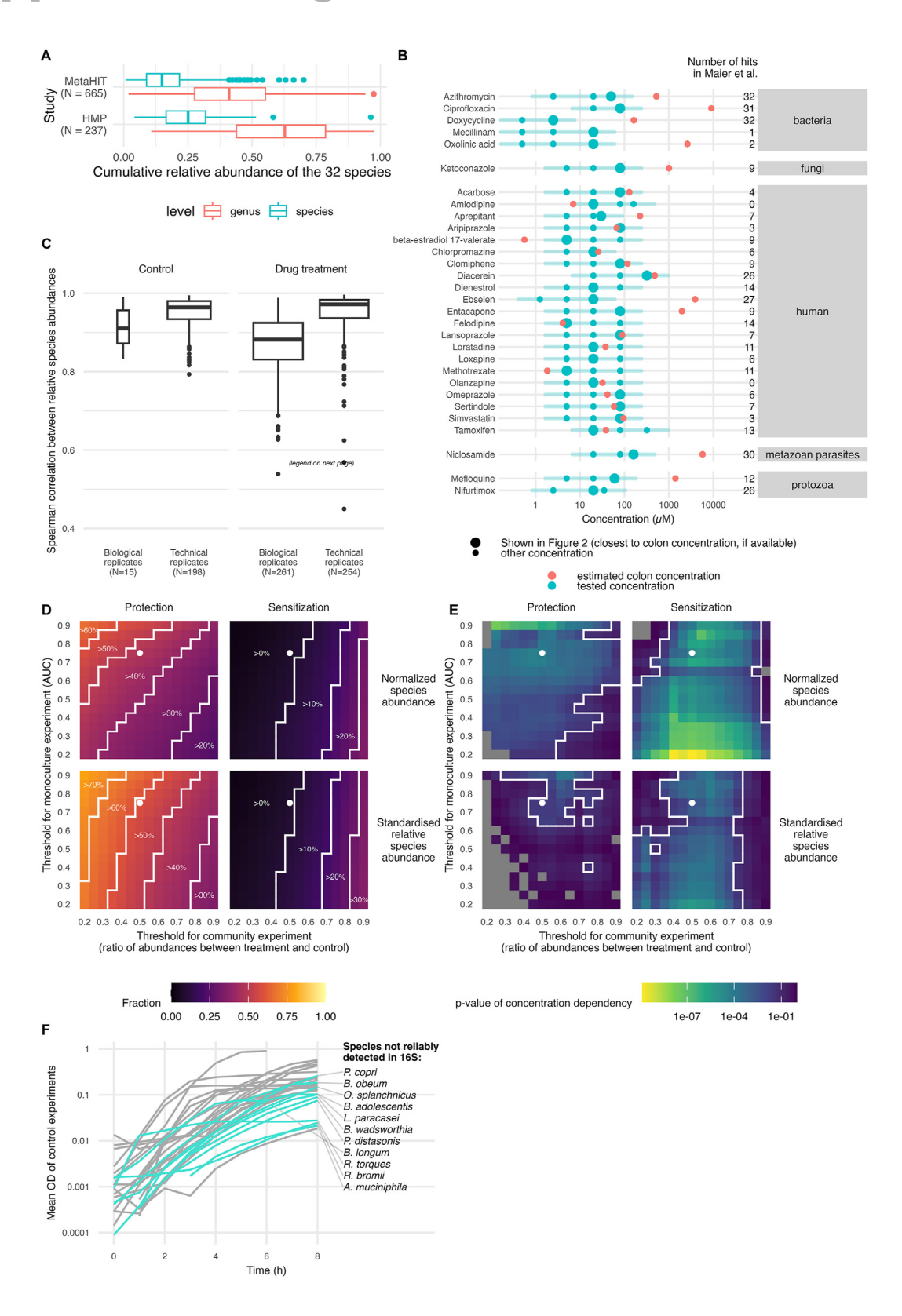






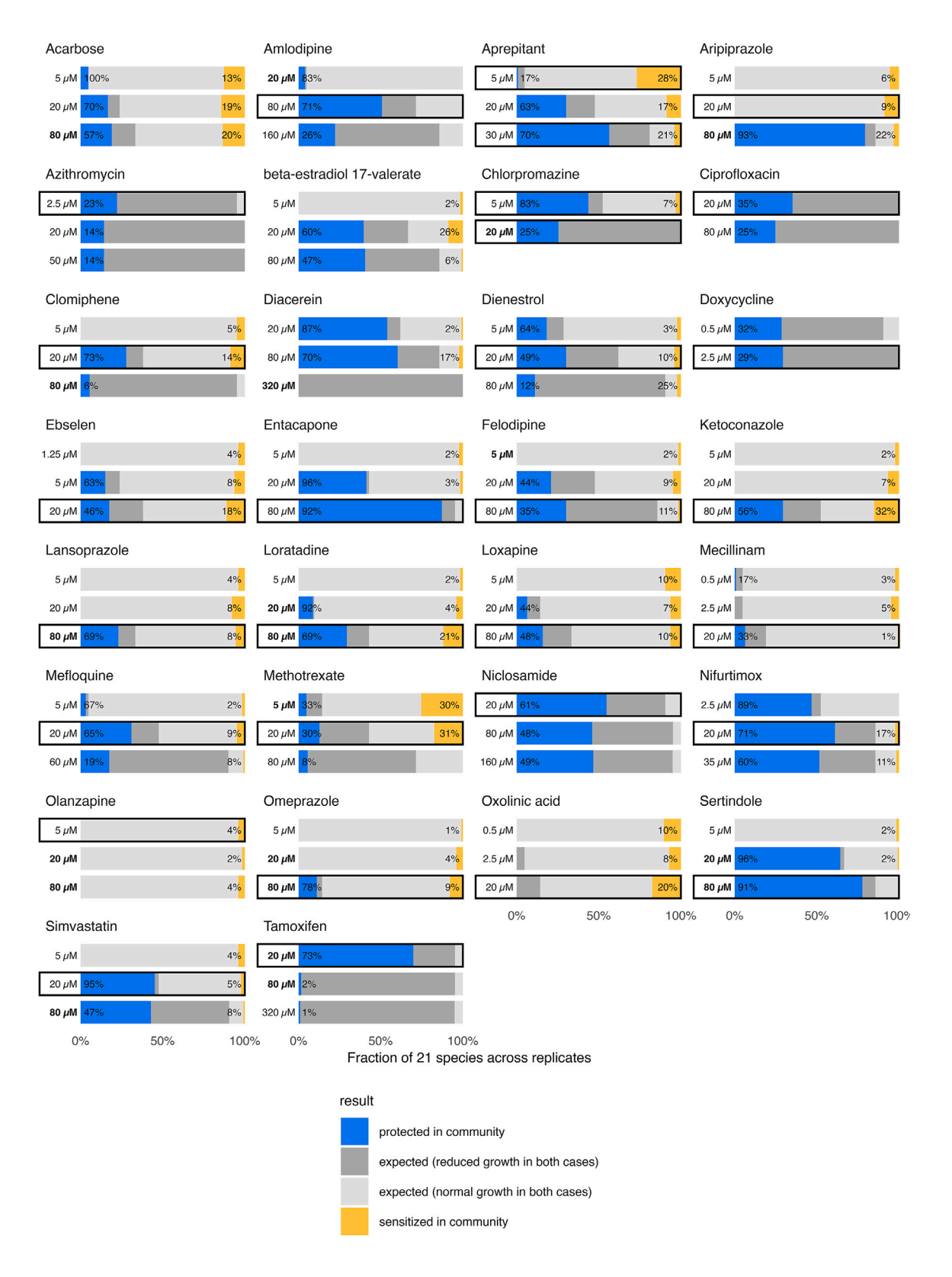
Figure S1. Characteristics of strains and drugs selected, quality control, and threshold exploration for screen, related to Figure 1

(A) Coverage of tested species in fecal samples. The tested 32 species were mapped against gut microbiome data from the Human Microbiome Project¹⁴ (HMP) and MetaHIT. ¹⁵ The median of the combined relative species abundance of the tested species was 25% in HMP and 15% in MetaHIT. Counting genera from which at least one species was tested here, 63% and 41% were covered, respectively. The boxplots represent the distribution of the data, and summary statistics and outliers as described in Figures 2D and 2E.

- (B) The drug concentrations tested in the screen. Selection was based on prior knowledge of drugs' activity at $20 \mu M^3$ (counts of species targeted on the right side). Estimated colon concentrations are shown as a red dot (when available), and tested concertation closest to the estimated colon concentration is shown as enlarged dots (if colon concentration is not available, then the $20 \mu M$ is shown).
- (C) Distribution of Spearman correlations between relative abundances for technical and biological replicates for 16S sequencing. The boxplots represent the distribution of the data, and summary statistics and outliers as described in Figures 2D and 2E.
- (D) Exploration of thresholds for defining growth inhibition in the community and in monoculture. Cells are colored by the fraction of protected (left) or sensitized (right) species for pairs of thresholds. The white dot designates the chosen thresholds of 25% growth inhibition in monoculture and 50% growth inhibition in the community. White lines delineate regions of similar fractions. The fractions of protection and sensitization changed only slowly as the cutoffs for determining growth inhibition were varied. Likewise, the abundance normalization based on OD produces similar results as the standardization of relative abundances by dividing by the 75th percentile of relative abundances.
- (E) The concentration dependency of the fraction of protection and sensitization is not sensitive to the chosen thresholds of defining growth inhibition. The white line encloses the region where the *p* value of the concentration dependency is below 0.05 (calculated as in Figure S3). Gray cells are shown for threshold pairs where the sigmoid curve fitting for the concentration dependency failed.
- (F) Growth curves of the 32 species that constituted the community, using data from Maier et al.³ The mean optical density (OD) over time in hours (h) is shown in log scale. Highlighted in turquoise are the species that could not be consistently detected by 16S amplicon sequencing in the community setting in untreated conditions. Stains exhibiting slow growth rate and low yield are often, but not always, the ones absent from the community.







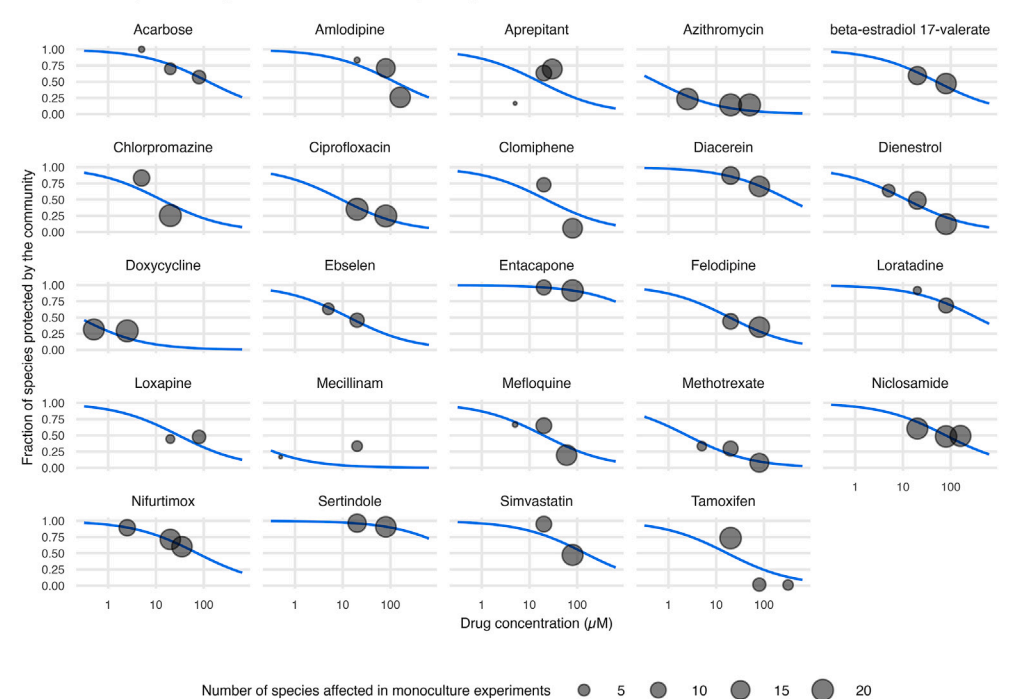




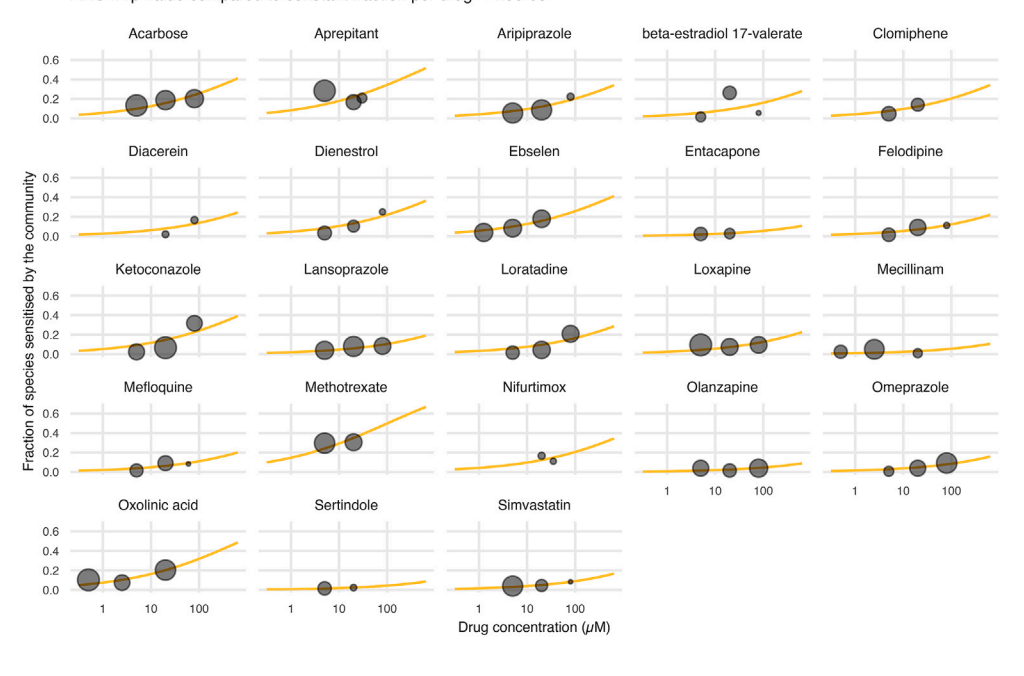




A Protection in community:
Logistic function with common growth rate and drug-specific offset
ANOVA p-value compared to constant fraction per drug = 7.2e-05



B Sensitization in community:
Logistic function with common growth rate and drug-specific offset
ANOVA p-value compared to constant fraction per drug = 1.9e-05



10 15

20

Number of species not affected in monoculture experiments





(A) The fraction of protected species is shown as a function of the drug concentration. We modeled the dependency between the drug concentration and the fraction of affected species as a logistic function, which has two parameters: the growth rate and the offset (i.e., the concentration where the fraction of the affected species would be 0.5). For the curve fitting, we used the same growth rate for all drugs, but drug-specific offsets. Hence, the "shape" of the logistic curve is the same across all drugs, but the curve is shifted according to the drugs' overall effect on the community. ANOVA was used to compare the logistic function fit to a concentration-independent model with a constant fraction of affected species per drug. (B) is same as (A), but this time for cross-sensitization.



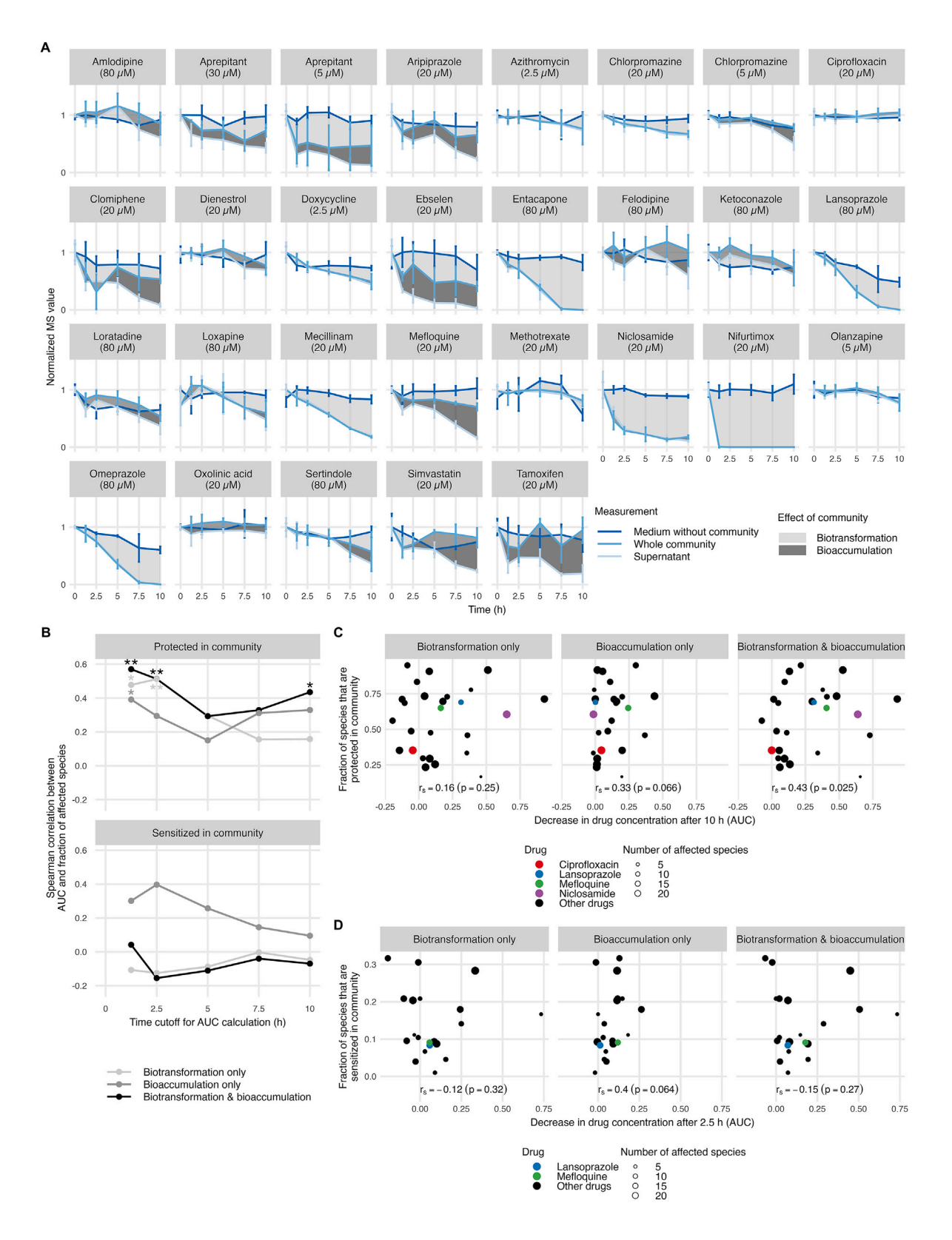






Figure S4. Metabolomics profiling of communities partially explains cross-protection, related to Figure 3

(A) Time course of biotransformation and bioaccumulation for all drugs (graphs plotted as in Figure 3A). The error bars represent the standard deviation of the replicates.

(B) The correlation between the compound biotransformation and/or bioaccumulation and the fraction of protected (top) and sensitized (bottom) species as a function of different time cutoffs in the metabolomics data. Asterisks: $^*rp < 0.01$, $^*p < 0.05$. p values were calculated by permutation tests using 100,000 samples. (C) Fraction of protected species in the community as a function of drug biotransformation and/or bioaccumulation at 10 h. Only biotransformation and bioaccumulation together show a significant correlation. p values were calculated as in (B).

(D) Fraction of sensitized species in the community as a function of drug biotransformation and/or bioaccumulation at 2.5 h. Only bioaccumulation shows some correlation, albeit it fails to reach significance—partially also due to the low number of bioaccumulation cases. p values were calculated as in (B).





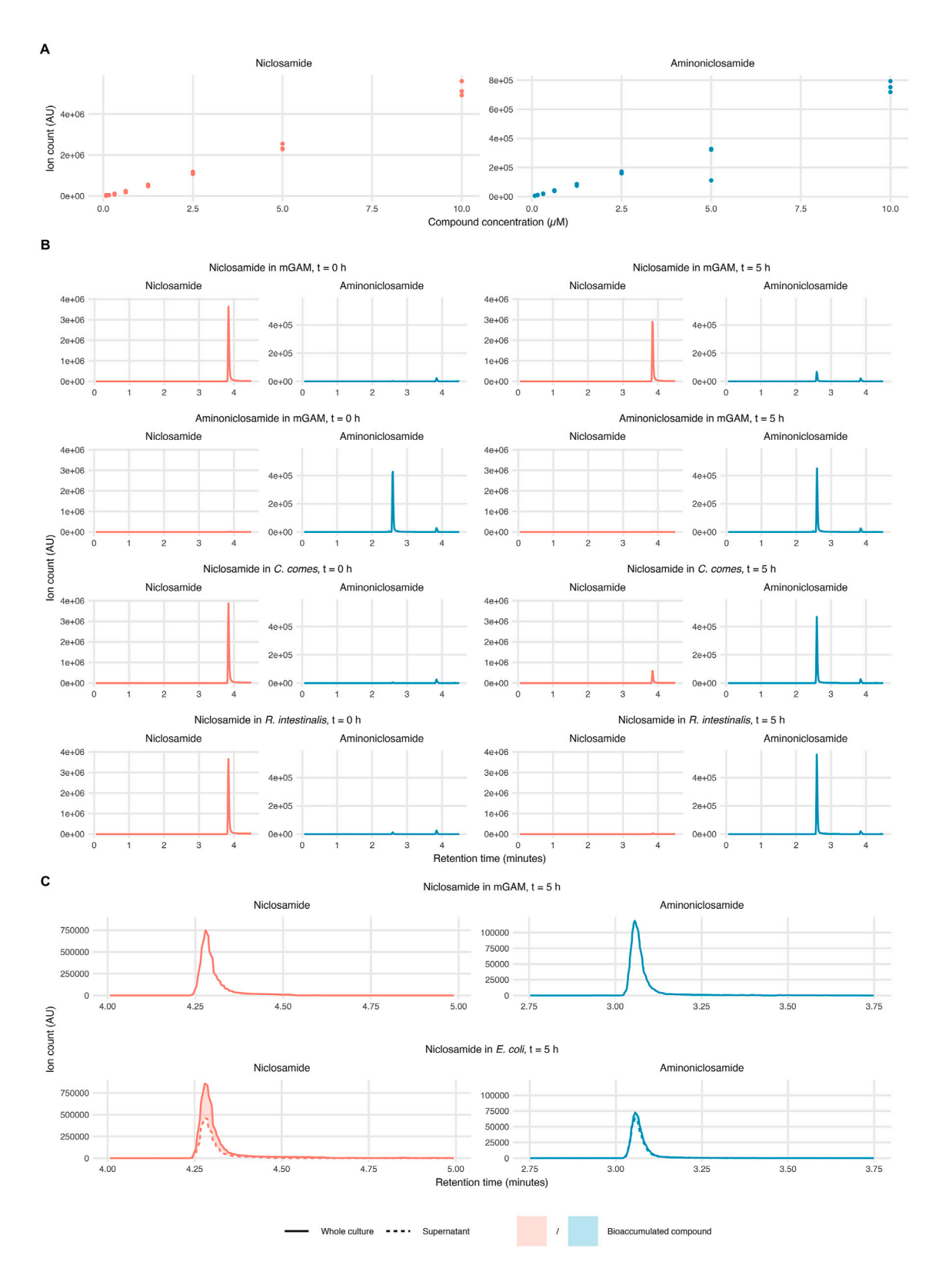






Figure S5. LC-MS traces for niclosamide and aminoniclosamide, related to Figure 4

(A) Calibration curves for niclosamide (left) and aminoniclosamide (right) were generated by pooling the two compounds in fresh mGAM and performing 1:2 serial dilutions, starting from a concentration of 10 μM down to 0.08 μM. The y axis shows the peak intensity corresponding to each concentration.

(B) Incubation of 10 μM niclosamide and aminoniclosamide in mGAM for 5 h shows that only a small fraction of niclosamide is converted to aminoniclosamide (top two rows). Both *C. come*s and *R. intestinalis* fully convert niclosamide to aminoniclosamide in 5 h (bottom two rows). Note that the peak intensity for aminoniclosamide after the incubation matches the one from the aminoniclosamide standard, indicating a stoichiometric conversion.

(C) Incubation of niclosamide (10 µM) with *E. coli* for 5 h (second row) exhibited lower turnover to aminoniclosamide than when niclosamide was incubated in media mGAM for same time (top row). At the same time, the concentration of niclosamide in the supernatant was lower than the concentration in the whole culture, indicating the *E. coli* has bioaccumulated niclosamide. Three biological replicates with two technical replicates each have been combined, calculating the mean across replicates and the moving average across five data points.





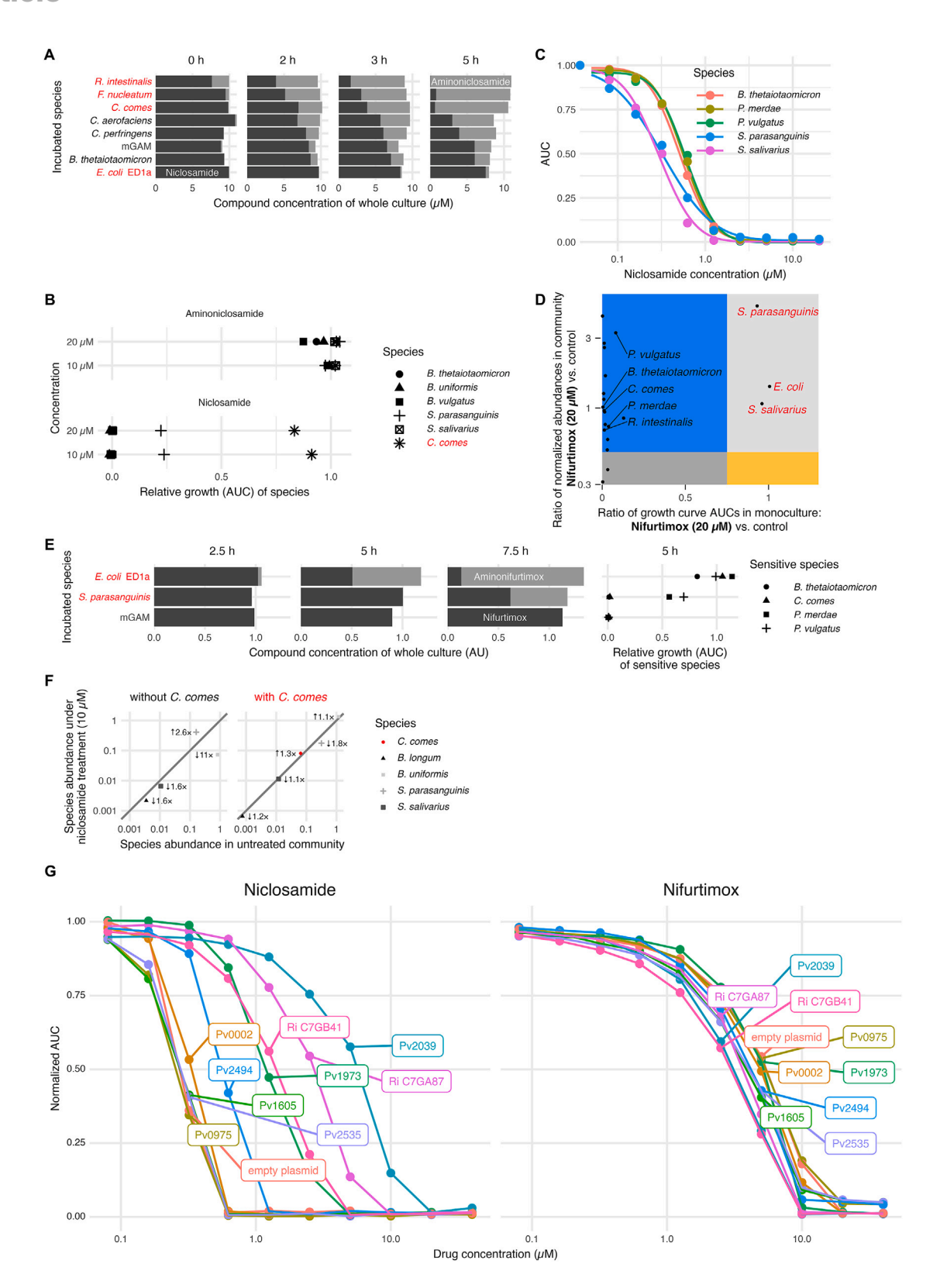






Figure S6. Contribution of individual strains to niclosamide and nifurtimox community protection, related to Figures 4 and 5

(A) Full time course for the niclosamide degradation experiment shown in Figure 4B.

- (B) Relative growth of niclosamide-sensitive (black) and resistant (red) species subjected to niclosamide (control) and aminoniclosamide treatments. Aminoniclosamide was non-toxic to all species.
- (C) Single-species growth under niclosamide treatment. For illustrative purposes, monotonic spline models were fitted to the AUC data points.
- (D) Single-species versus community growth phenotypes upon treatment with 20 μ M nifurtimox. Representation of species that grow in community as expected from monoculture (light and dark gray areas) or that are cross-protected (blue area) or cross-sensitized (yellow area) in the community.
- (E) Full time course for nifurtimox biotransformation (as in A). In contrast to niclosamide, *E. coli* strongly reduced nifurtimox to aminonifurtimox. Spent media from *E. coli* and *S. parasanguinis* (resistant species to nifurtimox; C), grown in the presence of 40 µM nifurtimox (or vehicle) for 5 h, was mixed 1:1 with fresh mGAM and used to grow nifurtimox-sensitive strains. Growth of the sensitive was normalized to their growth in spent media from untreated cultures.
- (F) Protection of the community under niclosamide treatment by *C. comes*. The same data as in Figure 4F is shown but as a scatter plot of relative abundances in control versus niclosamide treatment. Next to each species, the fold change and its direction are shown. In the community without *C. comes*, the abundances of the four species change by a factor of 3 on average. With *C. comes*, this is reduced to an average of 1.3.
- (G) Niclosamide and nifurtimox dose response curves for *P. vulgatus* heterologously overexpressing different nitroreductases. Although specific nitroreductases increased the dose response and IC₉₀ to niclosamide (Figure 5A), minor or no changes were observed for nifurtimox.